aerospace

MDPI

Article

Numerical Investigation and Parameter Sensitivity Analysis on Flow and Heat Transfer Performance of Jet Array Impingement Cooling in a Quasi-Leading-Edge Channel

Lei Xi, Jianmin Gao, Liang Xu *, Zhen Zhao, Qicheng Ruan and Yunlong Li

State Key Laboratory for Manufacturing Systems Engineering, Xi'an Jiaotong University, Xi'an 710049, China; xilei100@mail.xjtu.edu.cn (L.X.); gjm@mail.xjtu.edu.cn (J.G.); zhaozhen.900803@stu.xjtu.edu.cn (Z.Z.); ruanqicheng93@stu.xjtu.edu.cn (Q.R.); ylongli@mail.xjtu.edu.cn (Y.L.)

* Correspondence: xuliang@mail.xjtu.edu.cn; Tel.: +86-18691861949

Abstract: In this study, numerical simulations were carried out to investigate the flow and heat transfer characteristics of jet array impingement cooling in the quasi-leading-edge channel of gas turbine blades. The influence laws of Reynolds number (*Re*, 10,000 to 50,000), hole diameter-to-impingement spacing ratio (*d/H*, 0.5 to 0.9), hole spacing-to-impingement spacing ratio (*S/H*, 2 to 6), and Prandtl number (*Pr*, 0.690 to 0.968) on flow performance, heat transfer performance, and comprehensive thermal performance were examined, and the corresponding empirical correlations were fitted. The results show that increasing the *d/H* and reducing the *S/H* can effectively reduce the pressure loss coefficient in the quasi-leading-edge channel. Increasing the *Re*, reducing the *d/H*, and increasing the *S/H* can effectively enhance the heat transfer effect of the target wall. When *d/H* = 0.6 at lower Reynolds numbers and *S/H* = 5 at higher Reynolds numbers, the comprehensive thermodynamic coefficient reaches its maximum values. The average Nusselt numbers and comprehensive thermal coefficients of the quasi-leading-edge channel for steam cooling are both higher than those for air cooling. The pressure loss coefficient of the quasi-leading-edge channel is most sensitive to the change in *d/H* but is not sensitive to the change in *Re*. The average Nusselt number of the quasi-leading-edge channel is most sensitive to the change in *Re* and is least sensitive to the change in *Pr*. The comprehensive thermal coefficient of the quasi-leading-edge channel is most sensitive to the change in *Re*. The findings may provide a reference for the design of a steam-cooling structure in the leading edge channel of high-temperature turbine blades.

Keywords: blade leading edge; steam jet array; impingement cooling; flow and heat transfer; sensitivity analysis

Citation: Xi, L.; Gao, J.; Xu, L.; Zhao, Z.; Ruan, Q.; Li, Y. Numerical Investigation and Parameter Sensitivity Analysis on Flow and Heat Transfer Performance of Jet Array Impingement Cooling in a Quasi-Leading-Edge Channel. *Aerospace* **2022**, *9*, 87. https://doi.org/10.3390/aerospace9020087

Academic Editors: Qiang Zhang and Shaopeng Lu

Received: 24 January 2022
Accepted: 7 February 2022
Published: 9 February 2022

1. Introduction

The rotor inlet temperature of an advanced gas turbine is as high as 2000 K [1], which is far beyond the heat resistance limit of metal materials such as stainless steel and titanium. Consequently, effective cooling measures must be applied to gas turbine blades. The leading edge region of a turbine blade has the largest heat load [2], therefore the design of a cooling structure for a turbine blade leading edge needs more attention. Jet impingement cooling is one of the most effective methods to improve the local heat transfer coefficient [3] and is widely used in the cooling of the turbine blade leading edge.

In the study of impingement cooling, the impingement target walls have generally been simplified as flat walls to facilitate the research. A volume of research has been published regarding the flow and heat transfer performance of jet impingement on flat target walls. Experimental and numerical studies on jet impingement cooling are reported in a large number of works. Bradbury et al. [4] previously analyzed the velocity distribution of a typical single-hole jet and the attenuation of jet axial velocity. Kercher et al. [5] previously fitted the heat transfer correlation of a square array jet impinging on a flat target

wall related to Reynolds number, hole spacing, and hole diameter based on experimental data. Liu et al. [6] explored the influence law of a tangential jet on the impingement heat transfer of the turbine blade leading edge and pointed out that the heat transfer enhancement effect of tangential jet impingement cooling was mainly related to the nozzle position and Reynolds number of the jet. Long et al. [7] measured the flow vortex structure and heat transfer characteristics of an elliptical jet hole impacting a cylindrical convex target wall and obtained the distribution laws of momentum thickness and wall shear stress. Nguyen et al. [8] investigated the flow field distribution of an under-expanded jet impinging on a flat wall and pointed out that the impingement distance and pressure ratio have a great influence on the transition of energy-contained eddies and the large-scale flow structures generated by the jet impingement. Xu et al. [9] numerically studied the flow and heat transfer performance of a 45° angled swirling jet impinging on a flat wall and fitted the heat transfer correlation for the 45° angled swirling jet impinging cooling at $6000 \leq Re \leq 30{,}000$. Dutta et al. [10] reviewed the development trend of jet impingement cooling in gas turbine blades in recent years. They pointed out that the shapes of jet hole outlet, target wall, impingement channel, and the influence of cross-flow are the focus of current jet impingement cooling research. Deng et al. [11] studied the cooling performance of a wall jet with the advantages of swirl cooling and impingement cooling by using the conjugate heat transfer method. They stated that the overall cooling effectiveness of the wall jet cooling is 19% to 54% higher than that of the traditional methods for the cooling of a gas turbine blade. Yang et al. [12] researched the distribution characteristics of flow and heat transfer for a jet impingement cooling scheme with extended jet holes. Their results showed that the heat transfer effect and heat transfer uniformity of the extended jet holes are both better than those of the traditional jet impingement holes.

Although much work has been conducted on the flow and heat transfer performance of a jet impinging on flat target walls, because the wall surface of a turbine blade is curved, researchers began to pay attention to the research of jet impingement on concave target walls to improve the accuracy and practicability of impingement cooling for turbine blades. At present, many studies have also been carried out on the flow and heat transfer performance of a jet impinging on a concave target wall. Patil et al. [13] studied the effects of nozzle aspect ratio and target curvature on the flow and heat transfer characteristics of a jet impinging on a concave target wall and pointed out that small target curvature and large nozzle aspect ratio have the best comprehensive thermal performance when the heat transfer and pressure loss are comprehensively considered. Wang et al. [14] studied the heat transfer characteristics of a single-row jet impinging on a concave target wall of a turbine blade leading edge and found that the tangential jet provided more uniform heat transfer distribution than the conventional jet. Li et al. [15] experimentally investigated the flow behavior of sweeping jets impinging on a confined concave target wall and reported that the most important factors affecting flow behavior are the shape of the concave target wall and the inlet Reynolds number. Lyu et al. [16] examined the influence law of curvatures on the heat transfer capacity of a single-row chevron-jet impinging on concave walls. Their results showed that the influence level of concave curvature on the impingement heat transfer capacity of the chevron jet is significantly affected by the Reynolds number and impingement distance of the jet. Then, they [17] compared the heat transfer capacity of a tri-dimensional lobed jet impinging on a flat target wall and a concave target wall and pointed out that the stagnation heat transfer coefficient on the concave target wall is 20% to 30% lower than the flat target wall. Kura et al. [18] conducted a numerical investigation on the flow and heat transfer performance of single jet impingement on concave and convex target wall by using OpenFOAM (V9, ESI-OpenCFD Ltd, Bracknell, UK). They stated that the shape of the target wall affects the stagnation area size and leads to the difference in flow characteristics of jet impingement cooling. Xu et al. [19,20] studied and compared the heat transfer performance of swirling jet impingement cooling and circular hole jet impingement cooling on a semi-cylinder concave target by the large-eddy simulation method. They reported that the wall average Nusselt number of the 45° angled swirling jet impingement

cooling improves by 5% to 10% when compared with circular hole jet impingement cooling. Qiu et al. [21] conducted a numerical investigation on the flow and heat transfer features of jets impinging on a concave target wall with pin-fins. They stated that the existence of a pin-fin can effectively enhance the heat transfer capacity and heat transfer uniformity of the concave target wall. Tepe et al. [22] numerically studied the cooling performance of a staggered jet array impinging on a semi-circular concave target wall. They stated that lengthening the jet holes can effectively improve the heat transfer effect of the semi-circular concave target wall under the impingement of the staggered jet array. Forster et al. [23] researched the heat transfer effect of a jet impinging on the concave target wall of a gas turbine blade leading edge by using experimental and numerical methods. The results showed that the crossflow reduces the local Nusselt number of the stagnation point as well as the average Nusselt number of the target wall and increases the distribution uniformity of the local Nusselt number on the entire target wall.

In addition to the abovementioned flat and concave target walls, there are two important research topics in jet impingement cooling, these being turbulence model and cooling medium. For the turbulence model, this is very important for the accuracy of a numerical simulation of jet impingement cooling. Different turbulence models may lead to different calculation results. Therefore, it is necessary to select an appropriate turbulence model for the numerical simulation of jet impingement cooling. At present, the selection of a turbulence model for a numerical simulation of a jet impinging on a concave target wall has been examined by many investigators. Seifi et al. [24] used the k-w-v^2-f model to numerically study the heat transfer characteristics of a jet impinging on a concave target wall. The results show that the k-w-v^2-f model has better prediction performance than other models when the impingement distance is small. Hadipour et al. [25] studied the heat transfer and flow characteristics of a jet impinging on a concave target wall at a small impingement distance. They pointed out that the SST k-ω turbulence model can capture the distribution features of static pressure and heat transfer coefficient on the concave target wall well. Then, they [26,27] studied the influence of elliptical pin-fins on the flow and heat transfer performance of a circular hole jet impinging on a concave target wall; the results again proved the accuracy of the SST k-ω turbulence model in predicting the heat transfer performance of a jet impinging on a concave target wall. Huang et al. [28] reported that the modified SST k-ω turbulence model with the curvature correction can significantly improve the prediction accuracy of flow and heat transfer behaviors for the jet impinging on the concave target wall.

For the cooling medium, the physical properties of the medium have a great influence on the flow and heat transfer performance of jet impingement cooling. The more common media used for turbine blade cooling are air, steam, and mist. In the last decade, several studies have been carried out on the flow and heat transfer capacity of jet impingement cooling with different cooling mediums. Li et al. [29] and Wang et al. [30,31] proposed to apply the mist/steam jet impingement cooling to closed-loop steam-cooled gas turbine blades. They stated that the heat transfer effect of the steam jet with 0.5% mist impinging on a concave target wall is enhanced by up to about 200% at the stagnation point. Xu et al. [32] conducted a numerical study on the total steam jet impingement cooling of a gas turbine blade and pointed out that steam jet impingement cooling can effectively improve the cooling effect of a gas turbine blade. Alhajeri et al. [33] researched the heat transfer characteristics of mist/steam jet impingement on an unconfined target wall and reported that the addition of mist significantly improves the heat transfer capacity of the steam jet impingement cooling. Diop et al. [34] studied the heat transfer features of a jet impinging with a few amounts of mist. Their results showed that the average Nusselt number of the target wall for a jet with 3 mg/s and 6 mg/s mist is 21% and 32% higher than that of a jet without mist.

According to the above literature review, although much research has been devoted to the flow and heat transfer performance of a jet impinging on flat and concave target walls, little research has been conducted on the cooling performance of steam jet impingement

cooling for the leading edge of closed-loop steam-cooled gas turbine blades. Therefore, it is necessary to study the flow and heat transfer characteristics of steam jet impingement cooling in turbine blade leading edge channels and obtain the influence laws of structural parameters and working conditions on steam jet impingement cooling.

For the design of a steam-cooling structure of gas turbine blades, the authors of the present study previously carried out experimental and numerical studies on the cooling performance of a steam-cooled turbine blade of a heavy-duty gas turbine [32,35]. However, the cooling effectiveness of the leading edge region for the abovementioned blade was relatively poor. Therefore, further studies need to be carried out to solve the problems of poor cooling effect and high heat load of the leading edge channel in the steam-cooled gas turbine blade reported in the literature [32,35]. A feasible solution would be to arrange steam jet array impingement cooling in the leading edge channel of the abovementioned turbine blade.

The purpose of this study is to understand the flow and heat transfer characteristics of steam jet array impingement cooling in the quasi-leading-edge channel and obtain the influence laws of various parameters on the flow and heat transfer performance of the quasi-leading-edge channel. Therefore, in this study, a type of quasi-leading-edge channel with a jet array impingement cooling structure was established and simplified according to the blade's leading edge geometry. The flow and heat transfer characteristics of jet array impingement cooling in the quasi-leading-edge channel were analyzed in detail. The effects of Reynolds number (*Re*, 10,000 to 50,000), hole diameter-to-impingement spacing ratio (*d*/*H*, 0.5 to 0.9), hole spacing-to-impingement spacing ratio (*S*/*H*, 2 to 6), and Prandtl number (*Pr*, 0.690 for air to 0.968 for steam) on the flow and heat transfer performance of the quasi-leading-edge channel were discussed. The empirical correlations of pressure loss coefficients, heat transfer coefficients, and comprehensive thermal coefficients for jet array impingement cooling in the quasi-leading-edge channel were fitted within the parameters of the study. Finally, parameter sensitivity analysis of pressure loss coefficients, heat transfer coefficients, and comprehensive thermal coefficients to *Re*, *d*/*H*, *S*/*H*, and *Pr* was implemented. The results reveal the flow and heat transfer characteristics as well as the influence laws of various parameters for jet array impingement cooling in the quasi-leading-edge channel. The findings may provide a reference for the design of a steam-cooling structure in the leading edge channel of high-temperature turbine blades.

2. Research Object

2.1. Physical Model

In this investigation, the impingement cooling structure was designed for the leading edge channel of a steam-cooled gas turbine blade proposed by our research team [32,35]. The structural diagram of the steam-cooled gas turbine blade is shown in Figure 1a. The height, pitch, and chord length of this turbine blade were 83 mm, 96.4 mm, and 126 mm, and the installation angle and exit angle were 35.7° and 17°, as introduced in reference [35]. For the convenience of research and application, the leading edge channel of the steam-cooled gas turbine blade was taken out separately and simplified appropriately. The simplified leading edge channel, i.e., the quasi-leading-edge channel, is shown in Figure 1b. The quasi-leading-edge channel consists of a semi-cylindrical concave wall, two straight walls on both sides, and a bottom wall. The diameter of the semi-cylindrical concave was 9 mm, the length of the two straight walls was 9.5 mm, and the length of channel *L* was 40 mm. A plug-in channel was placed in the quasi-leading-edge channel to arrange the jet holes and act as the coolant supply plenum. The shape of the plug-in channel was the same as the shape of the quasi-leading-edge channel. The plug-in channel was connected to the bottom wall of the quasi-leading-edge channel through a stiffener. Due to the space limitation of the leading edge channel in the gas turbine blade, the jet impinging distance *H* was selected as 1 mm. Therefore, the calculated equivalent diameter *D* of the plug-in channel was 9 mm. Five columns of jet holes were arranged equidistantly along the channel circumference on the semi-cylindrical concave wall, and the angle between two adjacent columns of jet holes

was 45°. Two columns of jet holes were arranged at equal intervals on each of the two straight walls, and the distance between two adjacent columns of jet holes was 3 mm. The process of jet array impingement cooling is as follows: the cooling medium enters from the inlet of the plug-in channel, then it impinges and cools the wall of the quasi-leading-edge channel through the jet array holes on the plug-in channel, and finally, it flows out from the outlet of the quasi-leading-edge channel. During the study, the jet hole diameter d and the axial jet hole spacing S were changed to analyze the flow and heat transfer performance of the quasi-leading-edge channel and obtain the optimal configuration of the jet array impingement cooling structure. Due to the difficult processing, the easy blockage of jet holes, and the high strength requirements of the real gas turbine blade, the jet hole diameter, and jet hole spacing should not be too small. Meanwhile, due to the requirements of high cooling effect and low pressure loss of the real gas turbine blade, the jet hole diameter and jet hole spacing should not be too large. Therefore, based on the jet hole diameter and jet hole spacing of the impingement cooling structure of a real gas turbine blade, the jet hole diameter and jet hole spacing in this study were selected as 0.5 mm to 0.9 mm and 2 mm to 6 mm, respectively. Then, the impinging distance H was used to perform the dimensionless treatment on the parameters d and S. The dimensionless d/H and S/H ranged from 0.5 to 0.9 and from 2 to 6, respectively, which are also similar to the parameters used in most of the literature.

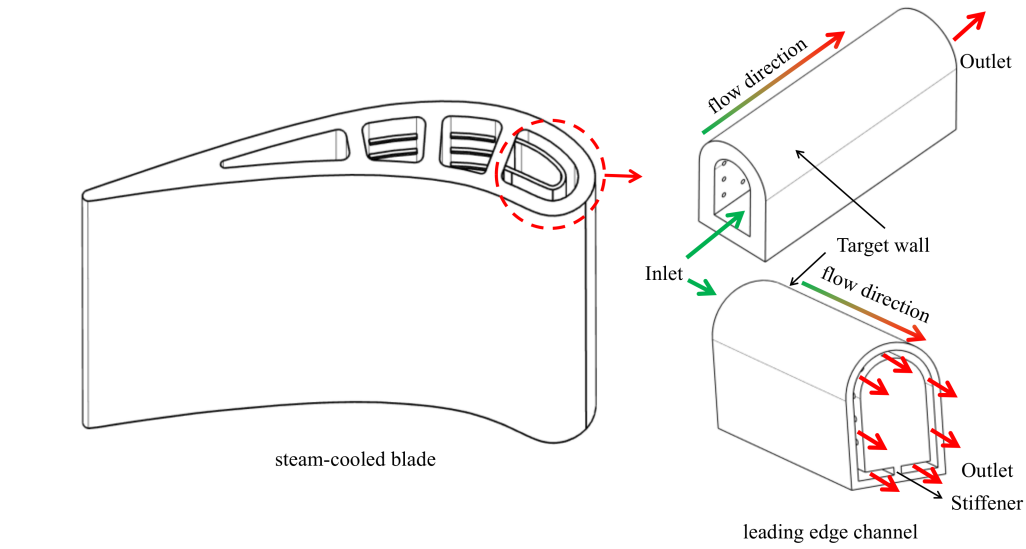

Figure 1. Research object: (**a**) the steam-cooled gas turbine blade; (**b**) the simplified leading edge channel.

2.2. Data Reduction

The inlet Reynolds number *Re*, which directly reflects the cooling flow rate of the blade leading edge channel, can be expressed as:

$$Re = uD/v \tag{1}$$

where u is the inlet velocity of the coolant; v is the kinematic viscosity of the coolant.

The wall Nusselt number *Nu* can be written as:

$$Nu = qD/[(T_w - T_{in})\lambda] \tag{2}$$

where q is the heat flux of the target wall; T_w is the temperature of the target wall; T_{in} is the inlet temperature of the coolant; λ is the thermal conductivity of the coolant.

The pressure loss coefficient C_p of jet array impingement cooling in the quasi-leading-edge channel can be defined as:

$$C_p = 2(p_{in} - p_{out})/\rho u^2 \tag{3}$$

where p_{in} is the channel inlet average pressure; p_{out} is the channel outlet average pressure.

Generally, for the internal cooling design of a gas turbine blade, higher heat transfer performance under equal pump power (i.e., under equal ${C_p}^{1/3}$) is hoped to be obtained. At the same time, in general, the pressure loss coefficient increases with the increase in wall Nusselt number. Therefore, a comprehensive coefficient is needed to evaluate the comprehensive thermal performance of the internal cooling channel. Consequently, the comprehensive thermal performance coefficient G, which is the ratio of *Nu* and ${C_p}^{1/3}$, was defined to comprehensively consider the flow and heat transfer performance of jet array impingement cooling in the quasi-leading-edge channel in this study. The expression of G can be written as:

$$G = Nu/{C_p}^{1/3} \tag{4}$$

3. Numerical Methods

3.1. Numerical Model

The numerical calculation model of jet array impingement cooling in the quasi-leading-edge channel is demonstrated in Figure 2. For the convenience of research, the stiffener that has little effect on the flow and heat transfer of the quasi-leading-edge channel was removed in the numerical model. As shown in Figure 2a, the calculation domain of the numerical model mainly includes the fluid in the plug-in channel, the jet array, and the fluid in the quasi-leading-edge channel. The cooling steam or air in the plug-in channel flows through the jet holes and impinges on the target wall heated by constant heat flux. In order to eliminate the calculation problems caused by the backflow at the outlet, a 40 mm long transition channel was added at the outlet of the quasi-leading-edge channel. Then, the calculation domain was divided into hexahedral-structured grids by the ICEM software, as shown in Figure 2b. The grid near the wall was refined to simulate the flow and heat transfer phenomena in the boundary layer. The height of the first layer of the near-wall grid was 0.001 mm, the growth ratio of the near-wall grid was 1.2. This grid generation strategy can ensure that the $y+$ value near the wall is less than 1, as required by the turbulence models of standard k-ω and SST k-ω. The grids of the jet holes and their surrounding area were also refined to improve the accuracy of the simulation for jet array impingement cooling. Moreover, the same grid strategy was used in the coupling surfaces of each calculation domain to minimize the transfer error.

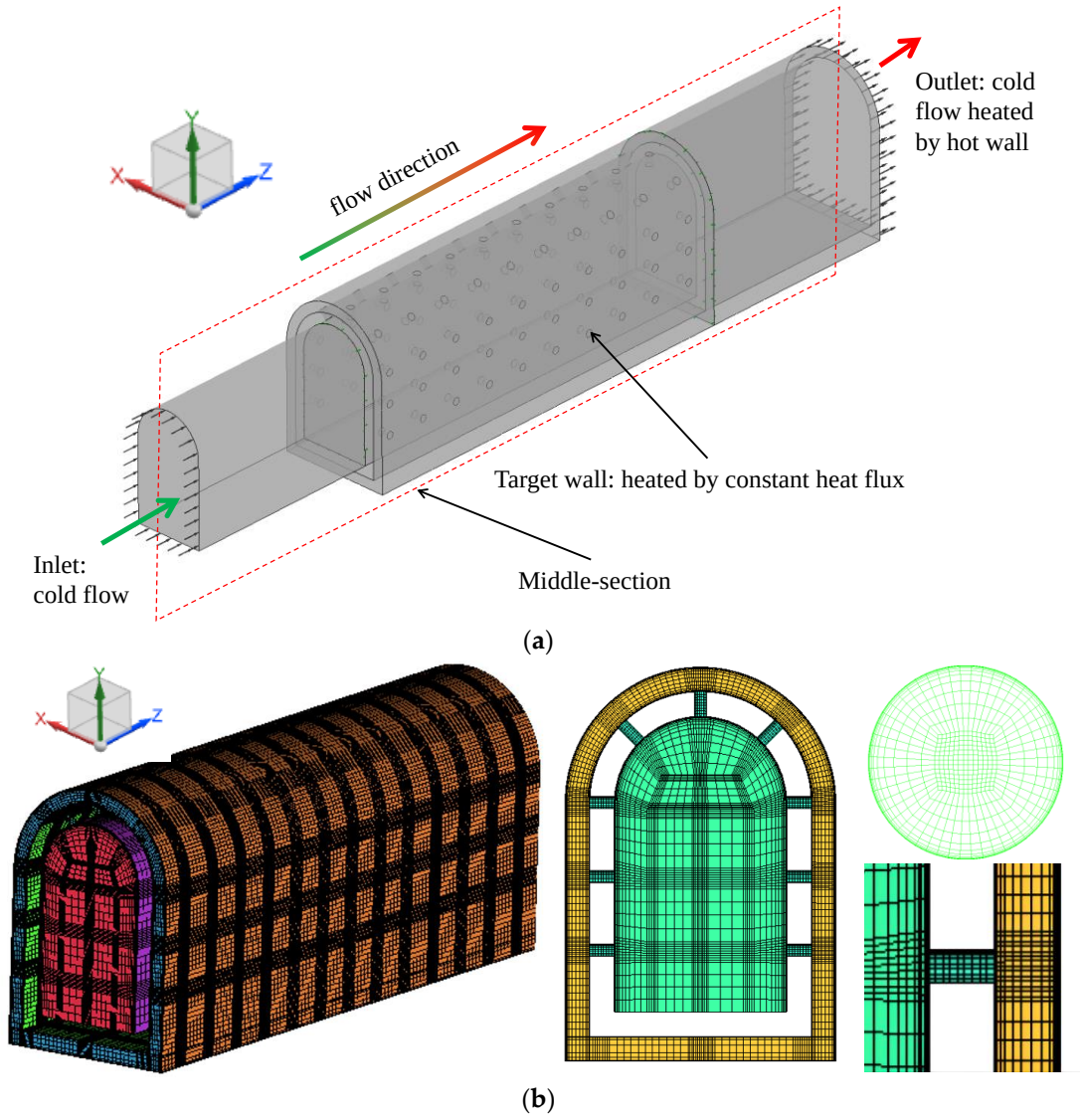

Figure 2. Numerical calculation model: (**a**) numerical model; (**b**) grid model.

Verification of grid independence was executed to guarantee the reliability and economy of the numerical methods for the simulation of jet array impingement cooling in the quasi-leading-edge channel. Six sets of grids were divided for the calculation model; the total grid numbers were 2.0 million, 2.6 million, 3.2 million, 3.8 million, 4.4 million, and 5.0 million, respectively. The values of the parameters selected for the grid independence verification were Re = 30,000, d/H = 0.7, S/H = 4. The results of grid independence verification are shown in Figure 3. As can be seen from Figure 3, when the total grid number is small, the average Nusselt number of the target wall increases with the increase in the total grid number. When the total grid number reaches about 4.4 million, the change in the average Nusselt number on the target wall is very small. This indicates that the requirement of grid independence is satisfied when the total grid number reaches 4.4 million. Therefore, the same grid generation strategy as the third set of grids with a total grid number of 4.4 million was adopted for different configurations of jet holes in the quasi-leading-edge channel in this study.

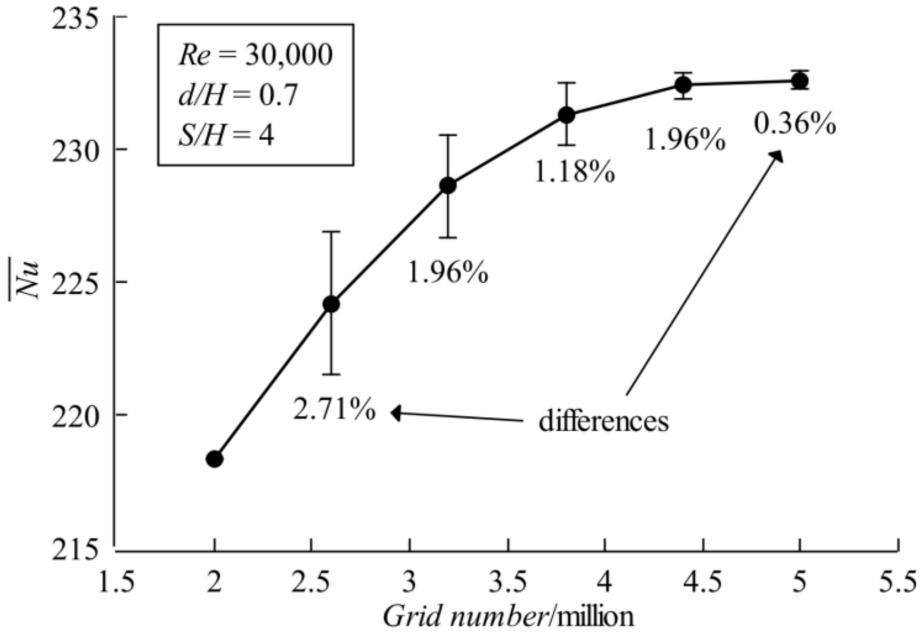

Figure 3. Verification of grid independence.

3.2. Numerical Calculation Method

In this investigation, the flow and heat transfer characteristics of jet array impingement cooling in the quasi-leading-edge channel were simulated by CFX software. The cooling fluid in the quasi-leading-edge channel was assumed to be 3D, compressible, and free of gravity. The governing equations were discretized by the bounded central difference scheme of the finite difference method. The Reynolds-averaged Navier Stokes equations were solved based on the fully implicit coupled multigrid. The High Resolution Scheme was selected for the options of Advection Schemes and Turbulence Numerics in the CFX-Pre [1]. The turbulent transport in the channel was simulated by different turbulence models, such as RNG k-ε, standard k-ω, and SST k-ω. The physical properties of the cooling steam were modified according to the IAPWS-IF97 material library. The physical properties of the cooling air were modified by the fitted correlation $c_p = 0.2348T + 936.95$ for specific heat capacity, and the Sutherland formulae $\lambda = \lambda_0(T/T_0)^{3/2}(T_0 + Su)/(T + Su)$ for thermal conductivity and $\mu = \mu_0(T/T_0)^{3/2}(T_0 + Su)/(T + Su)$ for dynamic viscosity. In the Sutherland formulae, Su is the Sutherland constant of 110.56 K and T_0 is the reference temperature of 273.16 K for λ_0 and μ_0. The condition for stopping the numerical simulation is that the residual level of each item converges below 10^{-6}.

The corresponding governing equations [1,36] are as follows.

The continuity equation:

$$\frac{\partial \rho}{\partial t} + \nabla \cdot (\rho \boldsymbol{U}) = 0 \tag{5}$$

The momentum equation:

$$\frac{\partial (\rho \boldsymbol{U})}{\partial t} + \nabla \cdot (\rho \boldsymbol{U} \otimes \boldsymbol{U}) = -\nabla p + \nabla \cdot \tau + \boldsymbol{S}_M \tag{6}$$

where τ is the stress tensor.

The total energy equation:

$$\frac{\partial (\rho h_{\text{tot}})}{\partial t} - \frac{\partial p}{\partial t} + \nabla \cdot (\rho \boldsymbol{U} h_{\text{tot}}) = \nabla \cdot (\lambda \nabla T) + \nabla \cdot (\boldsymbol{U} \cdot \tau) + \boldsymbol{U} \cdot \boldsymbol{S}_M + \boldsymbol{S}_E \tag{7}$$

where h_{tot} is the total enthalpy.

The form of advection schemes is:

$$\phi_{ip} = \phi_{up} + \theta \nabla \phi \cdot \Delta \vec{r} \quad (8)$$

where *ip* is the integration point; *up* is the upwind node; $\vec{r}$ is the vector from *up* to *ip*. Different θ and $\nabla\phi$ results in different schemes. When θ is close to 1, the advection schemes have a high resolution.

According to the experimental conditions in reference [32,35], the boundary conditions for jet array impingement cooling in the quasi-leading-edge channel were set as follows. The uniform velocity calculated by the Reynolds number of 10,000 to 50,000 and the total temperature of 474 K were assigned to the inlet of the plug-in channel. The turbulence intensity of the coolant at the inlet was set as 5%. The average static pressure of 244 kPa with a pressure fluctuation of 5% was assigned to the outlet of the quasi-leading-edge channel. The target wall of the quasi-leading-edge channel was set as the heated wall with a uniform heat flux of 10,000 $W \cdot m^{-2}$. The other walls were set as the adiabatic non-slip wall. In addition, the initialization conditions of the numerical simulation in this study were set as follows. For steam cooling, the initial inlet temperature and pressure were 474 K and 244 kPa, and the initial inlet normal velocity ranged from 15.90 $m \cdot s^{-1}$ to 79.51 $m \cdot s^{-1}$, according to the Reynolds number of 10,000 to 50,000. The density, specific heat capacity at constant pressure, thermal conductivity, dynamic viscosity, and Prandtl number of steam at channel inlet were 1.129 $kg \cdot m^{-3}$, 2.030 $kJ \cdot kg^{-1} \cdot K^{-1}$, 0.0339 $W \cdot m^{-1} \cdot K^{-1}$, 0.0000162 Pa·s, and 0.968, respectively. For air cooling, the initial inlet temperature and pressure were also 474 K and 244 kPa, and the initial inlet normal velocity varied from 16.10 $m \cdot s^{-1}$ to 80.49 $m \cdot s^{-1}$, according to the Reynolds number of 10,000 to 50,000. The density, specific heat capacity at constant pressure, thermal conductivity, dynamic viscosity, and Prandtl number of air at channel inlet were 1.794 $kg \cdot m^{-3}$, 1.026 $kJ \cdot kg^{-1} \cdot K^{-1}$, 0.0387 $W \cdot m^{-1} \cdot K^{-1}$, 0.0000261 Pa·s, and 0.690, respectively.

3.3. Verification of Numerical Method

The experimental data of a single row of a circular jet impinging on the semi-cylindrical concave wall in reference [20] were used to verify the numerical method in this study. The parameters selected were Re = 10,000 and d/H = 0.2. Three turbulence models, RNG k-ε, standard k-ω, and SST k-ω, were used for the numerical simulations. Then, the numerical results were compared with the experimental data. Figure 4 shows the comparison results between the experimental values of local Nu on the target wall and the corresponding simulation values of local Nu calculated by the three turbulence models. It can be seen that the distribution trends of the local Nu on the target wall calculated by the three turbulence models are consistent with the distribution trend of the experimentally measured local Nu. However, in terms of prediction accuracy, the simulation values of local Nu calculated by the RNG k-ε and standard k-ω turbulence models are obviously lower than those of the experimentally measured local Nu. The maximum prediction deviations of the RNG k-ε and standard k-ω turbulence models are about 17.79% and 15.03%, respectively. While the simulation values of local Nu calculated by the SST k-ω turbulence model are very close to the experimental values [25–28], the maximum prediction deviation of the SST k-ω turbulence model is about 6.36%. The above results show that the numerical method with the SST k-ω turbulence model used in this study can accurately and reliably simulate the heat transfer characteristics of the jet impinging on the semi-cylindrical concave wall. Therefore, the SST k-ω turbulence model was adopted to calculate the flow and heat transfer performance of jet array impingement cooling in the quasi-leading-edge channel in this investigation.

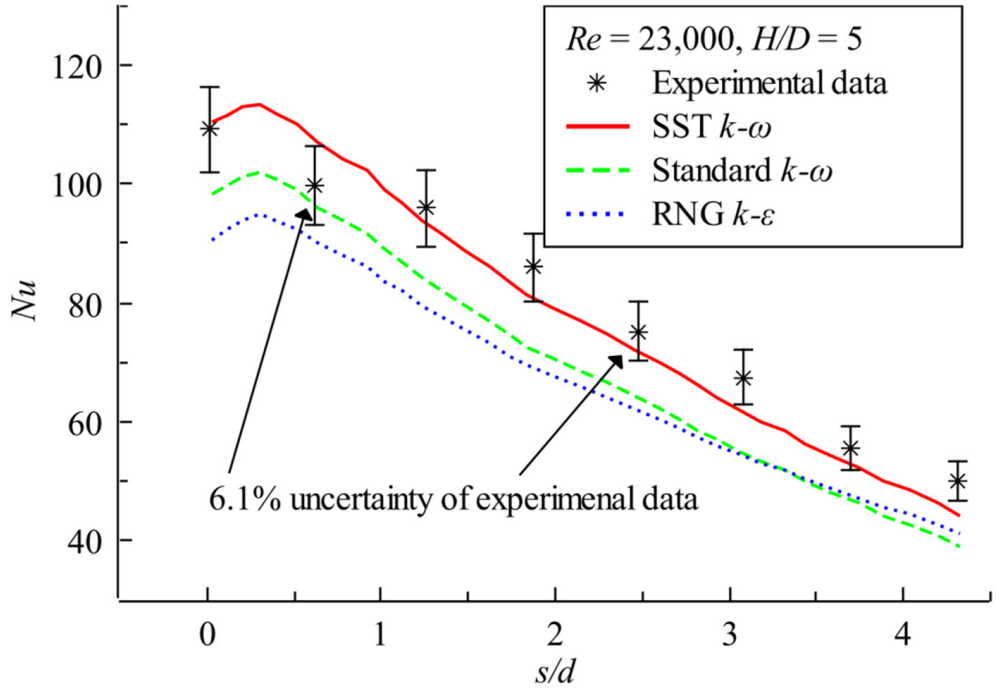

Figure 4. Validation of numerical methods.

4. Results Analysis and Discussion

4.1. Flow and Heat Transfer Characteristics

Figure 5 shows the flow field distribution of steam jet array impingement cooling in the quasi-leading-edge channel at Re = 30,000, d/H = 0.7, and S/H = 4, where Figure 5a is the three-dimensional flow field and Figure 5b is the two-dimensional flow field. As can be seen from Figure 5a, the flow field distribution in the impinging area of each row of jet holes is very similar along the circumferential direction of the channel but changes greatly along the axial direction of the channel. For the first two rows of jet holes near the entrance of the channel, the flow field distribution in the impinging area of each hole is similar to the flow field distribution in the core impinging area of the typical single-hole jet impingement cooling. That is, a symmetrical radial flow pattern is formed in the area between each jet hole and the target wall. With the development of the flow, from the third row of jet holes the flow field in the impinging area of each row of jet holes inclines downstream due to the influence of the axial flow of the upstream fluid. From the seventh row of jet holes, the flow field in the impinging area of each row of jet holes is completely distributed in the downstream area of the holes and displays a V-shaped pattern. At the same time, due to the increase in fluid from upstream, the fluid velocity in the core impinging area of the downstream rows of jet holes continuously increases. Then, the fluid velocity of the impinging jets near the outlet of the channel reaches the maximum. As can be seen from Figure 5b, two vortexes of the same size are formed on both sides of the first row of jet holes, and both vortexes are close to the target wall. Due to the extrusion of vortexes downstream of the first row of jet holes, a large vortex away from the target wall is formed upstream of the second row of jet holes. Meanwhile, a small vortex away from the target wall is formed downstream of the second row of jet holes under the influence of the transverse flow formed by the fluid of the first row of jet holes flowing along the channel axial direction. Due to the influence of the transverse flow formed by the fluid of the front rows of jet holes, the jet flows from the third row of holes to the fifth row of holes no longer vertically impinge the target wall, and the stagnation point of the jet impinging on the target wall moves downstream. Therefore, the vortexes formed upstream of the jet holes from the third row to the fifth row become smaller and smaller, and the vortex center of these vortexes also moves downstream. Meanwhile, the vortexes downstream of the jet holes from the

third row to the fifth row gradually disappear under the influence of transverse flow. From the sixth row of jet holes, the stagnation point of the impingement jet for each row of the holes continuously moves downstream, the vortexes upstream and downstream of the jet holes all gradually disappear, and the flow field distribution in this region of the channel becomes a simple inclined flow.

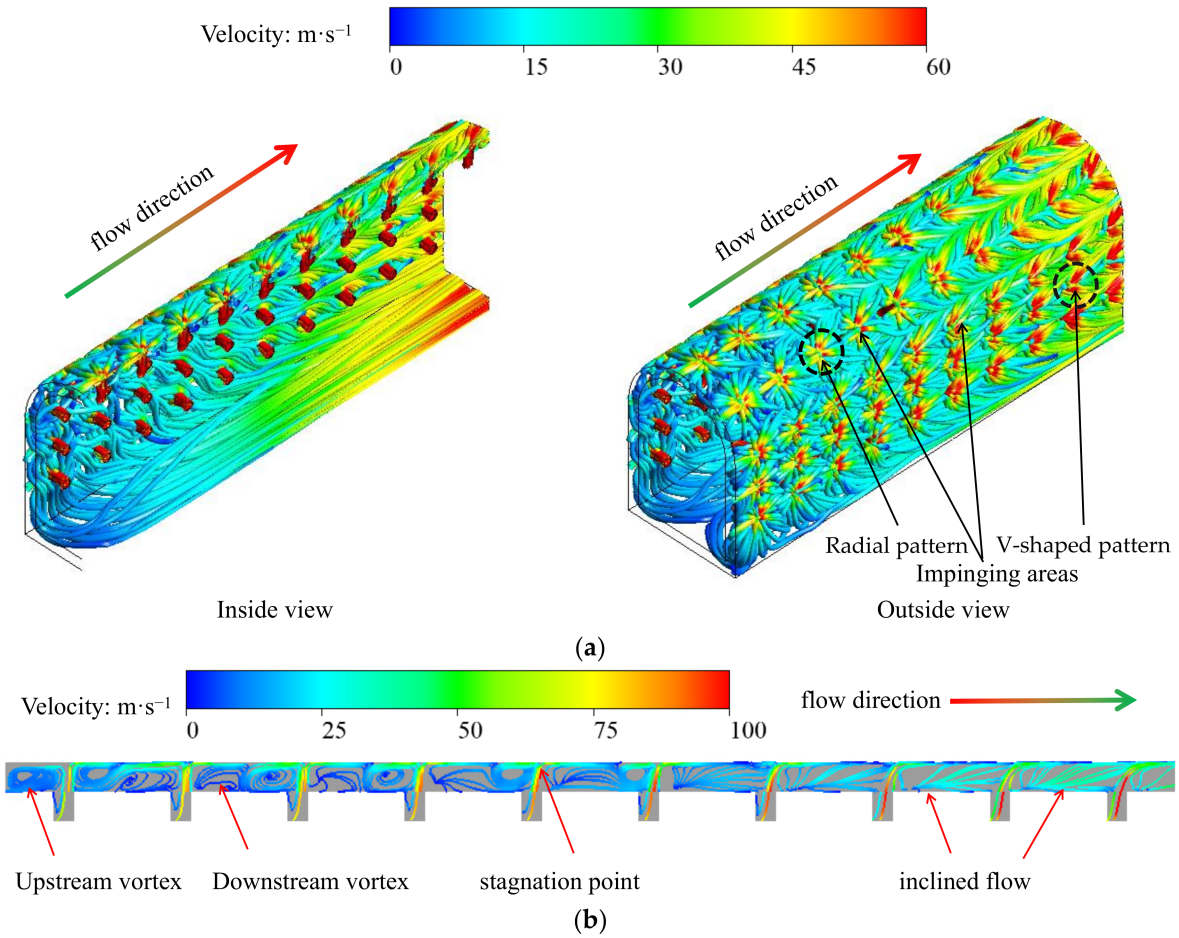

Figure 5. Flow field distribution characteristics of steam jet array impingement cooling in the quasi-leading-edge channel: (**a**) three-dimensional flow field; (**b**) two-dimensional flow field on the mid-section of the channel.

Figure 6 demonstrates the heat transfer distributions on the target wall of the quasi-leading-edge channel at Re = 30,000, d/H = 0.7, and S/H = 4 under steam cooling. On the whole, the heat transfer distributions on the target wall of the quasi-leading-edge channel present an array distribution in which the local Nusselt number in the stagnation area is high. The heat transfer distribution of jet array impingement cooling in the quasi-leading-edge channel is seriously affected by its flow field distribution. According to the analysis of the flow field distributions in Figure 5, the first two rows of impinging jets near the entrance of the channel impinge the target wall at a nearly perpendicular angle. Therefore, the first two rows of impinging jets yield high heat transfer regions with nearly circular pattern on the target wall. Then, with the increase in row number, the cross-flow formed by the front rows of impinging jets causes the back rows of impinging jets to not impinge the target wall vertically but incline downstream. Therefore, the pattern shape of the high heat transfer regions formed on the target wall downstream gradually becomes flat. In addition, due to the influence of the cross-flow formed by the upstream jets, the size of the high heat transfer region on the target wall gradually decreases along the axial direction of the channel, and the corresponding local heat transfer gradually weakens.

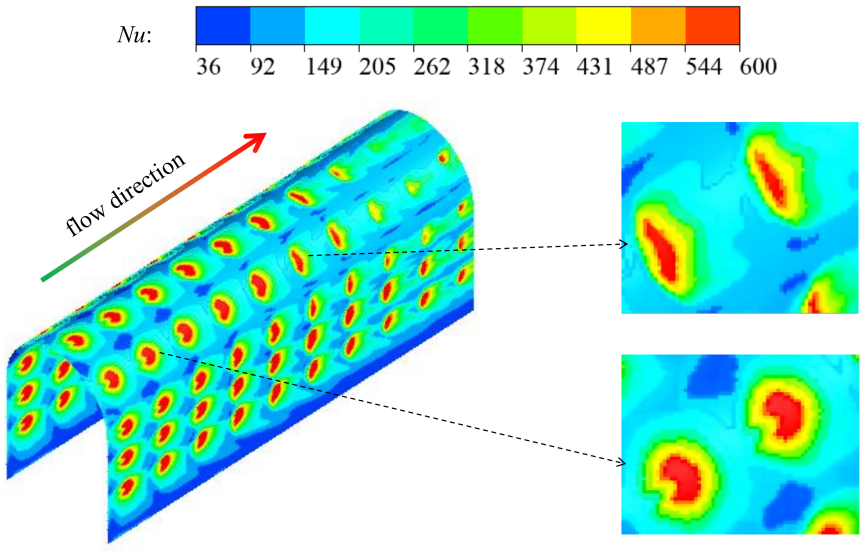

Figure 6. Heat transfer distribution characteristics of steam jet array impingement cooling in the quasi-leading-edge channel.

4.2. Effect of Reynolds Number

Figure 7 displays the flow field distributions and heat transfer distributions of steam jet array impingement cooling in the quasi-leading-edge channel under different *Re* at *d*/*H* = 0.7 and *S*/*H* = 4. As can be seen from the flow field distributions in Figure 7a, with the increase in Reynolds number, there is no obvious change in the flow field structure in the quasi-leading-edge channel; only the flow velocity at the corresponding position is significantly increased. As can be seen from the heat transfer distributions in Figure 7b, the local Nusselt number in each region of the target wall significantly increases with the increase in Reynolds number. This is because the jet velocity of each hole also increases with the increase in Reynolds number, which causes more heat to be taken away by the jet impinging on the target wall and then completely improves the heat transfer effect of the target wall. At the same time, the increase in the Reynolds number makes the attenuation speed of the high heat transfer area on the target wall weaker along the axial direction of the channel. This may be because the increase in jet velocity reduces the influence of the cross-flow from the upstream on the jet from the downstream.

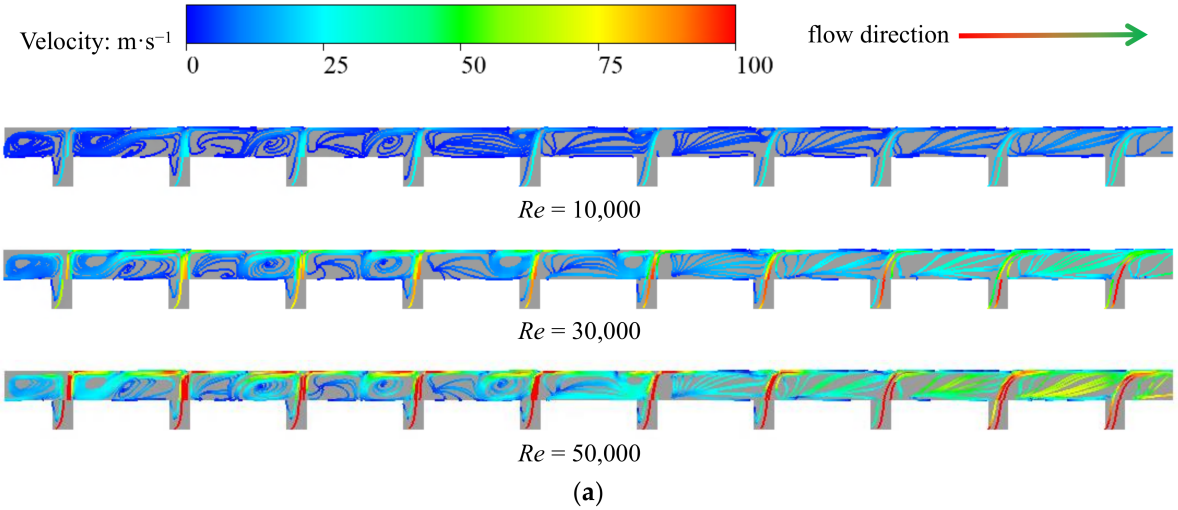

(**a**)

Figure 7. *Cont.*

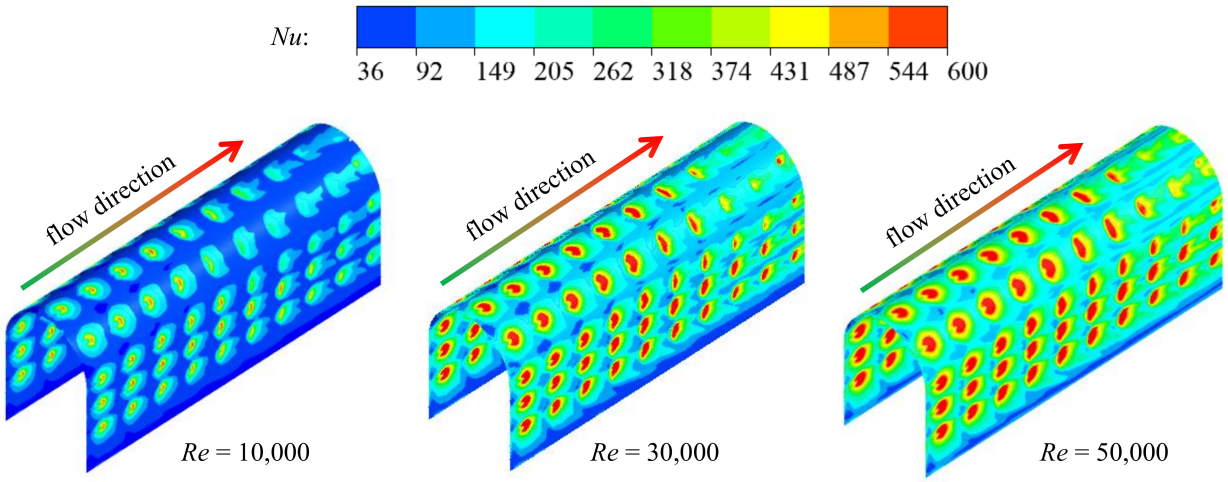

Figure 7. Distributions of flow field and heat transfer at different *Re* under steam cooling: (**a**) flow field distributions; (**b**) heat transfer distributions.

Figure 8 shows the effects of *Re* on the pressure loss coefficient, average Nusselt number, and comprehensive thermal coefficient of the quasi-leading-edge channel at *d*/*H* = 0.7 and *S*/*H* = 4 under steam cooling. It can be seen from Figure 8a that the change in *Re* has relatively little effect on the pressure loss coefficient of jet array impingement cooling in the quasi-leading-edge channel. The differences in the pressure loss coefficients are 2.4% to 6% when *Re* varies from 10,000 to 60,000 under different *d*/*H* and *S*/*H*. This is because the pressure loss coefficient is inversely proportional to the square of the inlet velocity and directly proportional to the pressure drop in the quasi-leading-edge channel, as shown in Equation (3). At the same time, the inlet velocity and the pressure drop both increase with the increase in *Re*, and the change rates of these with *Re* are close to each other. Thus, the change in the pressure loss coefficient with *Re* is very small. It can be observed from Figure 8b that, dissimilar to the effect of *Re* on the pressure loss coefficient of the quasi-leading-edge channel, the increase in *Re* can significantly improve the wall Nusselt number of jet array impingement cooling in the quasi-leading-edge channel. The quantitative result shows that the average Nusselt number of the quasi-leading-edge channel increases by 1.59 to 1.91 times under different *d*/*H* and *S*/*H* when *Re* increases from 10,000 to 60,000. It can be deduced from Figure 8c that the variation law of the comprehensive thermal coefficient with *Re* is different from that of the pressure loss coefficient with *Re* but is similar to that of the wall average Nusselt number with *Re*. That is, the increase in *Re* can effectively improve the comprehensive thermal performance of jet array impingement cooling in the quasi-leading-edge channel. The quantitative result shows that, when *Re* increases from 10,000 to 60,000, the comprehensive thermal coefficient of the quasi-leading-edge channel increases by 1.62 to 1.86 times under different *d*/*H* and *S*/*H*. In conclusion, increasing *Re* can greatly elevate the heat transfer effect and comprehensive thermal performance of jet array impingement cooling in the quasi-leading-edge channel but has little influence on the pressure loss coefficient of this channel.

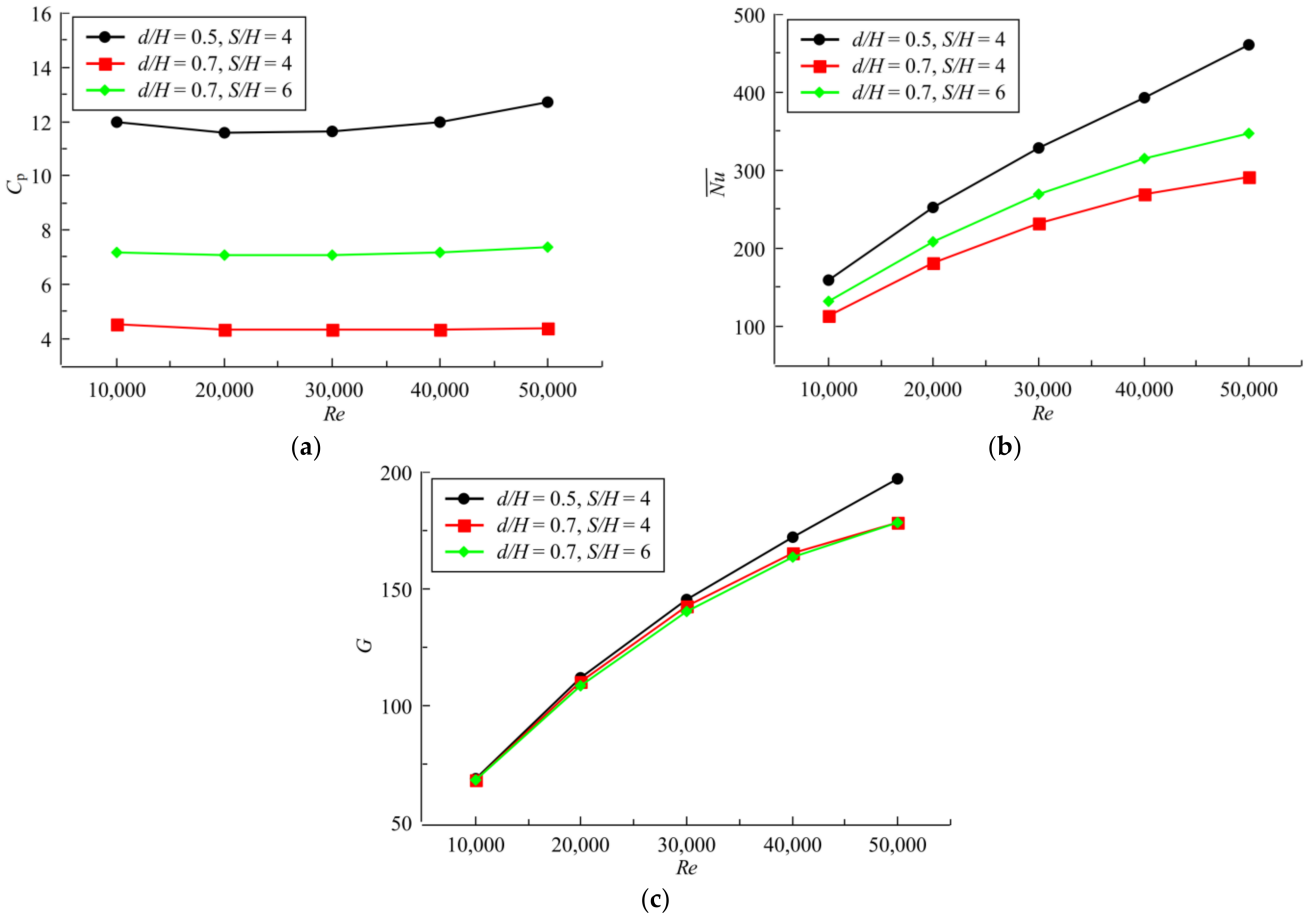

Figure 8. Effects of *Re* on the pressure loss coefficient, average Nusselt number, and comprehensive thermal coefficient of the quasi-leading-edge channel under steam cooling: (**a**) pressure loss coefficient; (**b**) average Nusselt number; (**c**) comprehensive thermal coefficient.

4.3. Effect of Jet Hole Diameter

Figure 9 illustrates the flow field distributions and heat transfer distributions of steam jet array impingement cooling in the quasi-leading-edge channel under different *d*/*H* at *Re* = 30,000 and *S*/*H* = 4. It can be seen from Figure 9a that the flow field distributions around the first four rows of jet holes are nearly the same for different jet hole diameters. From the fifth row to the seventh row of jet holes, the increase in the jet hole diameter makes the vortexes upstream of the jet holes gradually decrease in size or disappear in advance. From the eighth row of jet holes, the vortexes upstream and downstream of the jet holes almost all disappear. Moreover, the fluid velocity at the stagnation point gradually decreases with the increase in the jet hole diameter, which may weaken the heat transfer effect at the stagnation point. It can be seen from the heat transfer distributions in Figure 9b that with the increase in jet hole diameter, the local Nusselt number on the target wall significantly decreases and the number of impinging areas with a high heat transfer effect obviously decreases. This is because the increase in jet hole diameter reduces the jet velocity and weakens the scouring effect of the jet on the target wall, which worsens the heat transfer effect of the target wall.

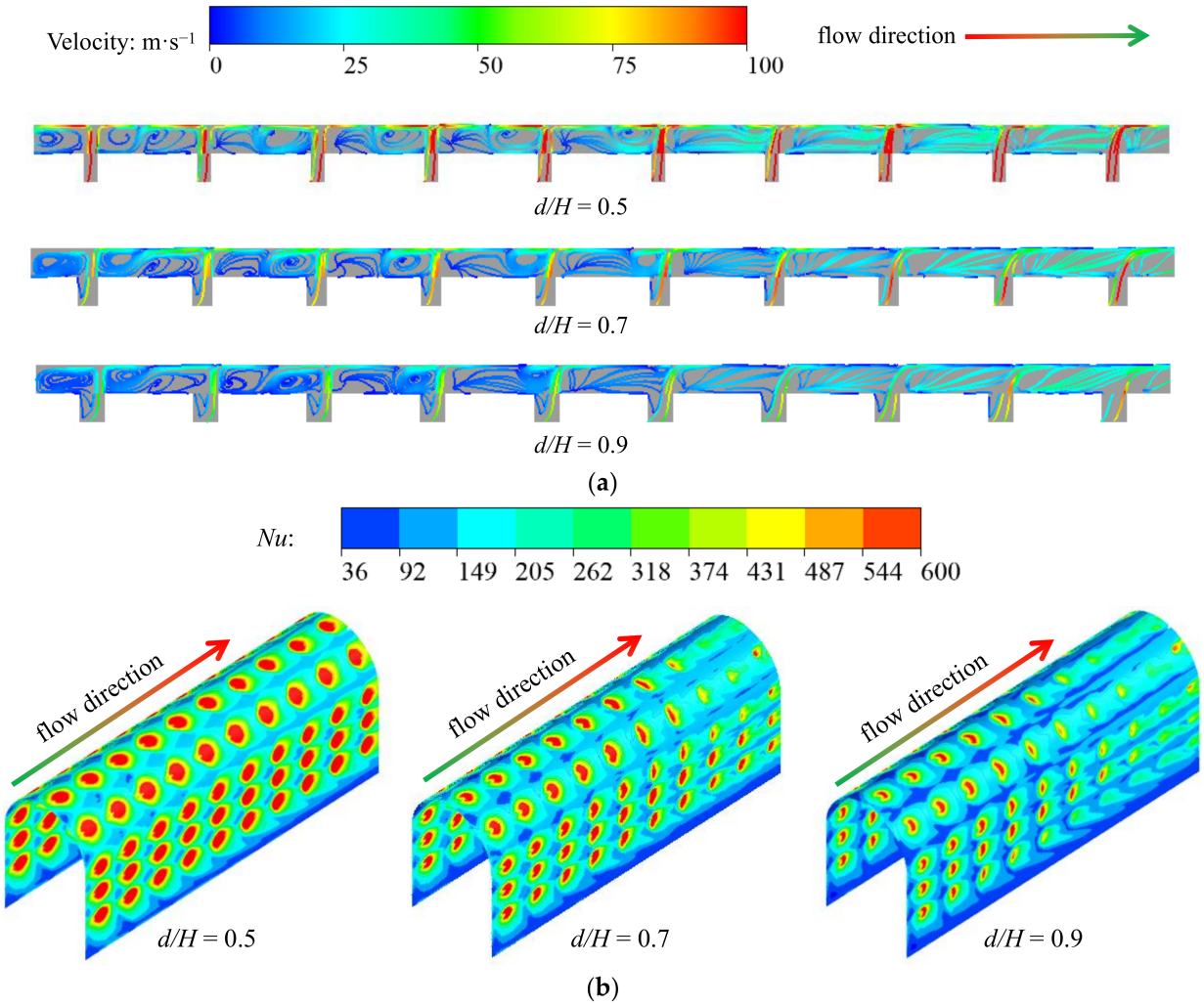

Figure 9. Distributions of flow field and heat transfer at different *d/H* under steam cooling: (**a**) flow field distributions; (**b**) heat transfer distributions.

Figure 10 displays the effects of *d/H* on the pressure loss coefficient, average Nusselt number, and comprehensive thermal coefficient of the quasi-leading-edge channel at *S/H* = 4 under steam cooling. It can be seen from Figure 10a that the pressure loss coefficient of the quasi-leading-edge channel is significantly reduced by increasing the *d/H* under various Reynolds numbers. This is because, as the *d/H* increases, the flow velocity at the jet stagnation point and its surrounding area significantly decreases, resulting in a decrease in local pressure loss in these areas. The calculation results show that the pressure loss coefficient of the quasi-leading-edge channel decreases by 76% to 79% when the *d/H* varies from 0.5 to 0.9 at different Reynolds numbers. It can be observed from Figure 10b that the increase in *d/H* significantly reduces the average Nusselt number of the target wall at various Reynolds numbers, and this trend is more obvious when the Reynolds number is higher. The quantitative results show that the average Nusselt number of the target wall decreases by 45% to 49% when the *d/H* increases from 0.5 to 0.9 at different Reynolds numbers. It can be deduced from Figure 10c that the comprehensive thermal coefficients of the quasi-leading-edge channel first increase and then decrease with the increase in *d/H* under lower Reynolds numbers, and they rapidly decrease with the increase in *d/H* under higher Reynolds numbers. It is worth noting that when the Reynolds number is low, the optimal value of *d/H* is 0.6, which makes the comprehensive thermal coefficients of the quasi-leading-edge channel reach the maximum values. In conclusion, increasing the jet hole diameter can effectively reduce the pressure loss coefficient of jet array impingement

cooling in the quasi-leading-edge channel; reducing the jet hole diameter can effectively enhance the heat transfer effect of the target wall of the quasi-leading-edge channel. The optimal value of *d*/*H* is 0.6 for improving the comprehensive thermal performance of the quasi-leading-edge channel at lower Reynolds numbers.

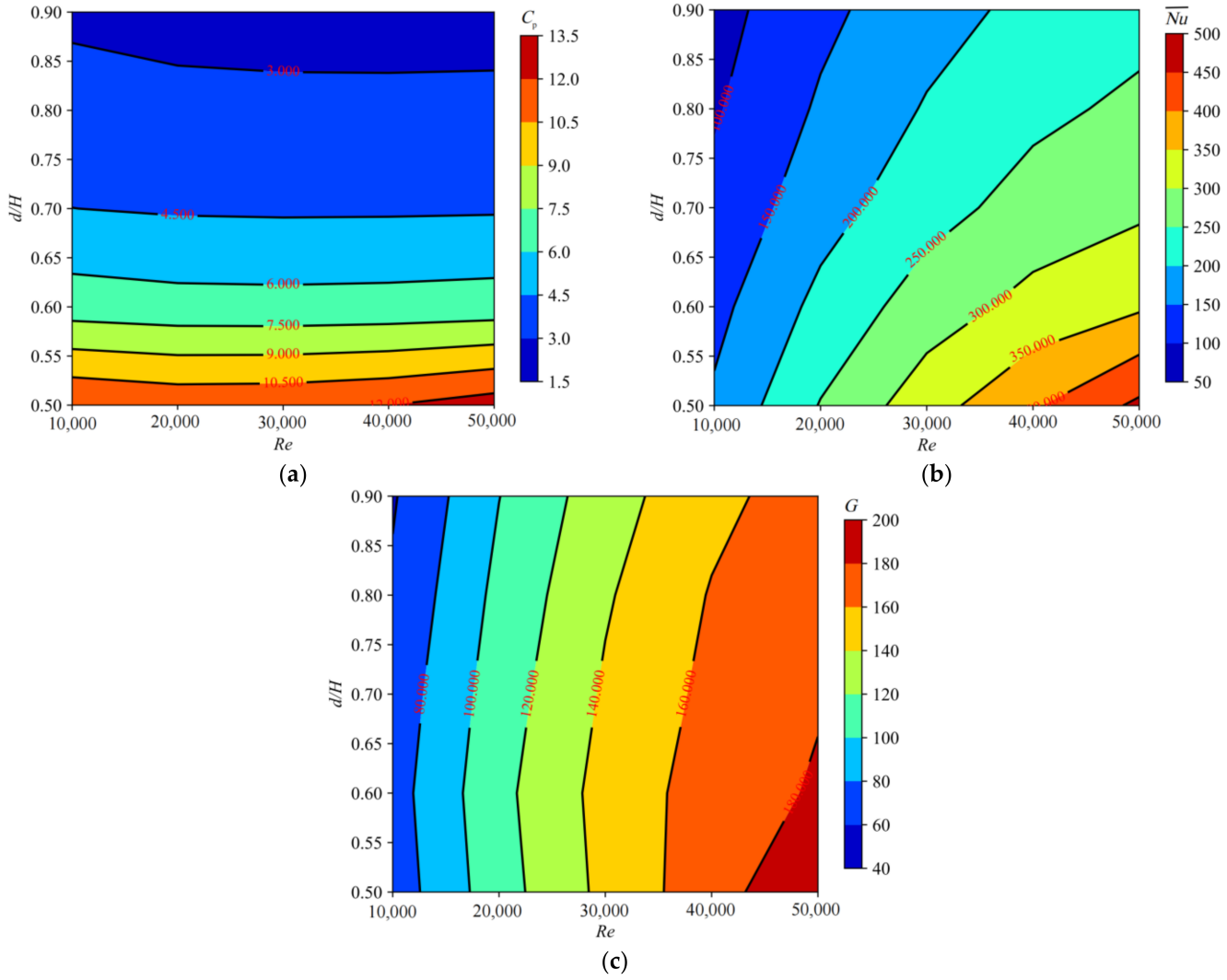

Figure 10. Effects of *d*/*H* on the pressure loss coefficient, average Nusselt number, and comprehensive thermal coefficient of the quasi-leading-edge channel under steam cooling: (**a**) pressure loss coefficient; (**b**) average Nusselt number; (**c**) comprehensive thermal coefficient.

4.4. Effect of Jet Hole Spacing

Figure 11 presents the flow field distributions and heat transfer distributions of steam jet array impingement cooling in the quasi-leading-edge channel under different *S*/*H* at *Re* = 30,000 and *d*/*H* = 0.7. As can be seen from the flow field distributions in Figure 11a, due to the constant channel length, increasing the hole spacing serves to reduce the number of jet hole rows that can be arranged along the axial direction of the channel. Although the number of jet hole rows changes at different hole spacings, the flow field distribution on the mid-section of the channel is similar under different hole spacings. The difference is that when the hole spacing is smaller, the size of the vortexes around the jet holes is smaller, the fluid velocity at the stagnation point is smaller, and the vortexes upstream of the jet holes disappear earlier along the axial direction. It can be seen from the heat transfer distributions in Figure 11b that with the increase in jet hole spacing, the number of high heat transfer areas on the target wall decreases but the size of each high heat transfer area

greatly increases. This is because the increase in jet hole spacing reduces the number of jet holes and increases the velocity of the jets, which improves the effect of impingement heat transfer of each jet on the target wall. On the whole, increasing the jet hole spacing improves the overall heat transfer effect of the target wall significantly.

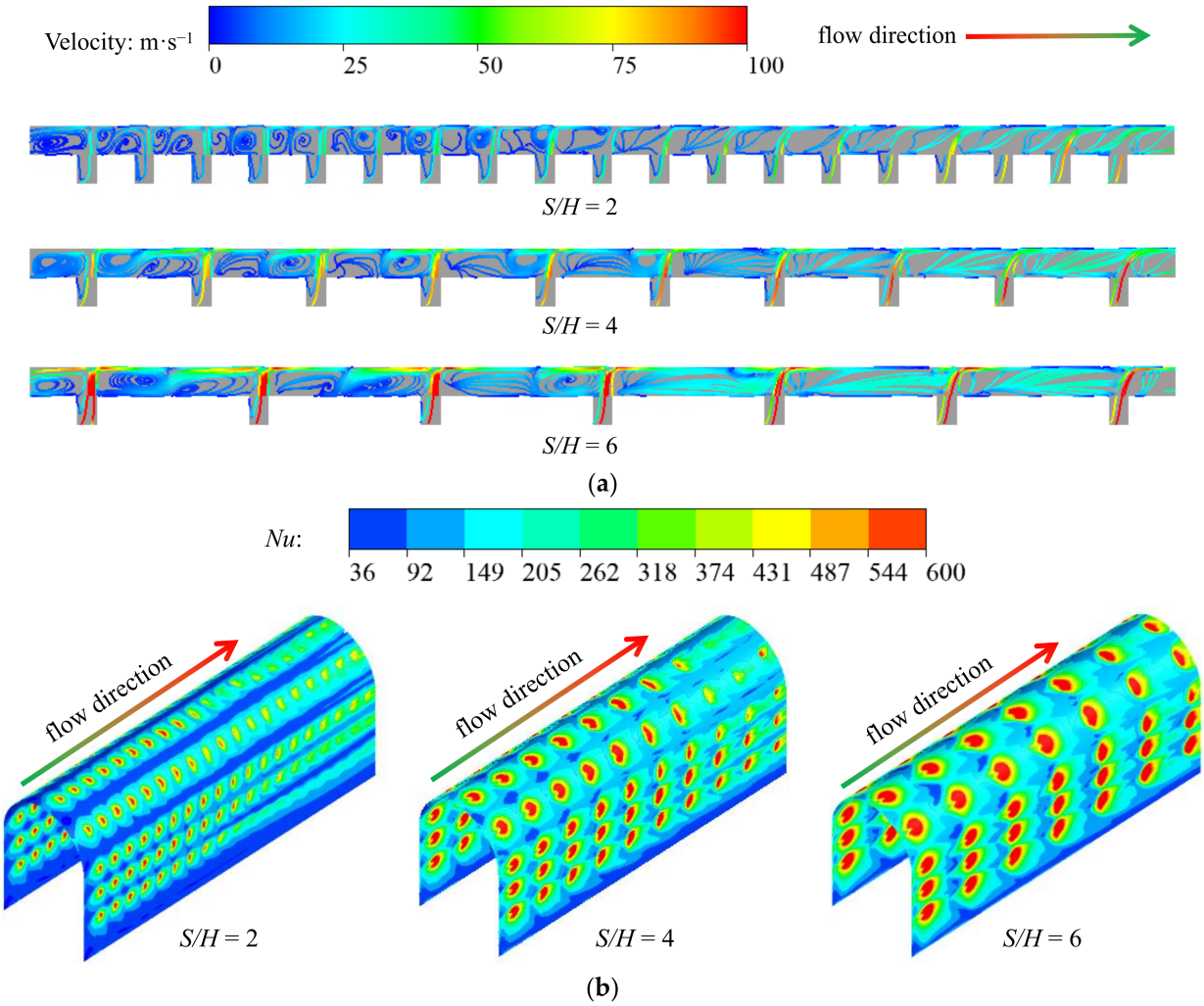

Figure 11. Distributions of flow field and heat transfer at different *S/H* under steam cooling: (**a**) flow field distributions; (**b**) heat transfer distributions.

Figure 12 presents the effects of *S/H* on the pressure loss coefficient, average Nusselt number, and comprehensive thermal coefficient of the quasi-leading-edge channel at *d/H* = 0.7 under steam cooling. It can be seen from Figure 12a that the pressure loss coefficient of the quasi-leading-edge channel increases with the increase in *S/H* at various Reynolds numbers. The reason is that the number of jet holes decreases with the increase in jet hole spacing, and the coolant velocity of each stagnation point and its surrounding area greatly increases. This results in the increase in local pressure loss in the impingement area, and then increases the whole pressure loss coefficient of the quasi-leading-edge channel. The calculation results show that the pressure loss coefficient of the quasi-leading-edge channel increases by 1.64 to 1.92 times when the *S/H* increases from 2 to 6 at different Reynolds numbers. Moreover, from the analysis of Figures 9a, 10a, 11a, and 12a, it can be concluded that the velocity of the coolant at the stagnation point and its surrounding area has the greatest influence on the pressure loss coefficient of the channel. It can be seen from Figure 12b that when the *S/H* is lower, the average Nusselt number of the target wall rapidly increases with the increase in *S/H*. When the *S/H* is higher, the average Nusselt

number of the target wall changes slowly, especially when the Reynolds number is lower than 20,000 and the *S/H* is higher than five; the average Nusselt number of the target wall remains basically unchanged along with the *S/H*. The quantitative results show that the average Nusselt number of the target wall increases by 54% to 64% when the *S/H* increases from 2 to 6 at different Reynolds numbers. As can be seen from Figure 12c, the comprehensive thermal coefficients of the quasi-leading-edge channel first increase and then remain unchanged with the increase in the *S/H* at lower Reynolds numbers, and they first increase and then decrease with the increase in the *S/H* at higher Reynolds numbers. When the Reynolds number is high, the comprehensive thermal coefficients of the quasi-leading-edge channel reach maximum values at *S/H* = 5. In summary, reducing the jet hole spacing can effectively reduce the pressure loss coefficient of jet array impingement cooling in the quasi-leading-edge channel, and increasing the jet hole spacing can significantly enhance the heat transfer effect of the target wall of the quasi-leading-edge channel. The optimal value of *S/H* for improving the comprehensive thermal performance of the quasi-leading-edge channel at higher Reynolds numbers is five.

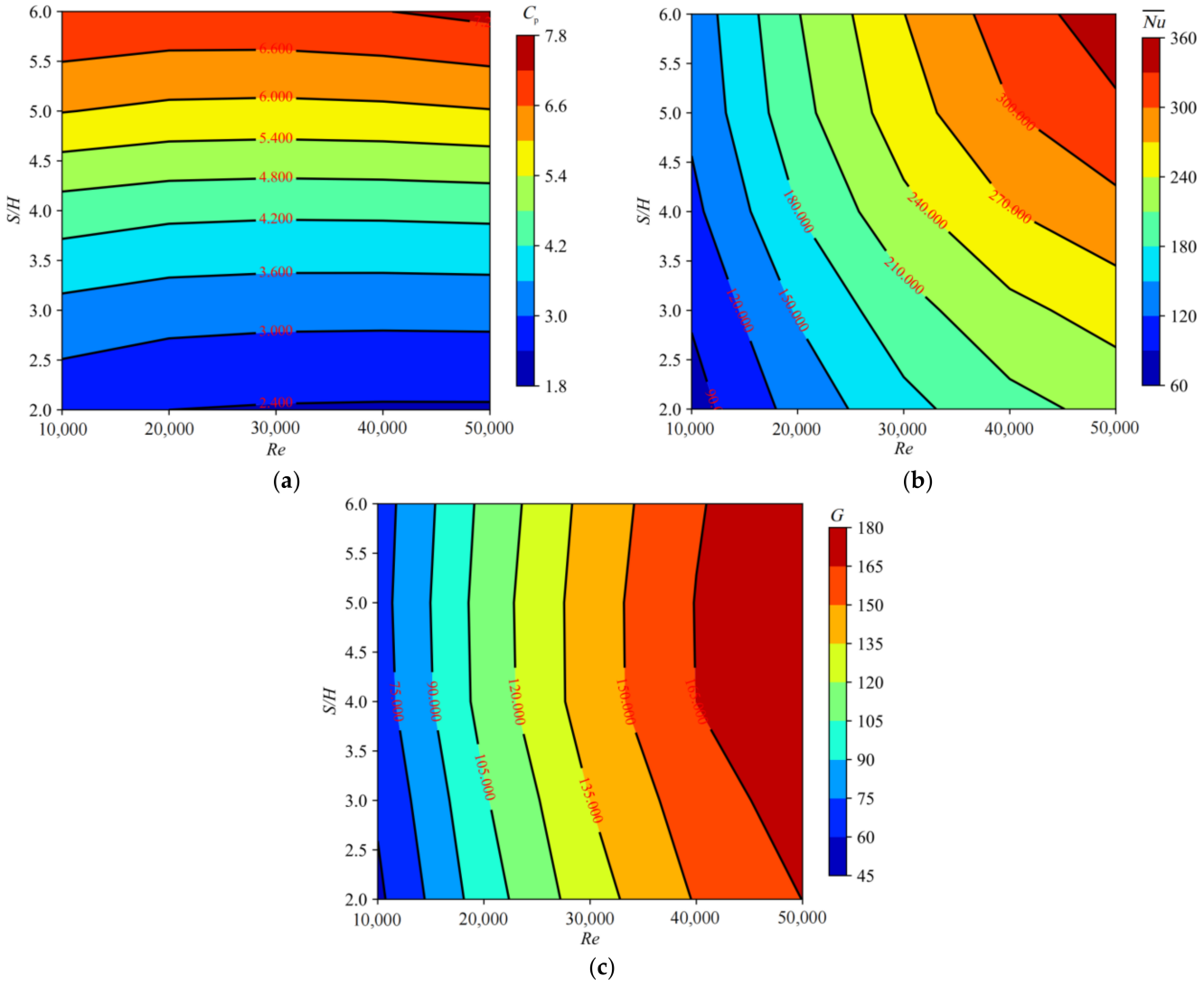

Figure 12. Effects of *S/H* on the pressure loss coefficient, average Nusselt number, and comprehensive thermal coefficient of the quasi-leading-edge channel under steam cooling: (**a**) pressure loss coefficient; (**b**) average Nusselt number; (**c**) comprehensive thermal coefficient.

In summary, the flow and heat transfer characteristics of jet array impingement cooling in the quasi-leading-edge channel with uniformly arranged jet holes of equal jet hole diameter were discussed in detail in Sections 4.1–4.4 in this study. In future research, the influence laws of non-uniform jet hole diameter and jet hole spacing on the flow and heat transfer performance of jet array impingement cooling in the quasi-leading-edge channel will additionally be studied in detail. This is because the issue of non-uniform jet hole diameter and jet hole spacing is interesting and meaningful for the application of jet array impingement cooling in the leading edge channel of turbine blades.

4.5. Comparison of Steam Cooling and Air Cooling

Figure 13 demonstrates the flow field distributions of jet array impingement cooling in the quasi-leading-edge channel under steam cooling and air cooling at Re = 30,000, d/H = 0.7, and S/H = 4. As can be seen in Figure 13a, the flow field structures of jet array impingement cooling in this channel for steam cooling and air cooling are very similar to each other. The difference is that the sizes of the counter-rotating vortex pairs formed on both sides of the first seven rows of jet holes for steam cooling are larger than those for air cooling. Meanwhile, the cores of those counter-rotating vortex pairs for steam cooling are farther away from the target wall when compared with air cooling. Additionally, the fluid velocity at the stagnation point and its surrounding area for air cooling is slightly higher than that for steam cooling. This is because the kinematic viscosity of air is greater than that of steam at the same temperature and pressure. This may result in a slightly higher pressure loss coefficient in the quasi-leading-edge channel for air cooling than for steam cooling. As can be seen in Figure 13b, the heat transfer distribution characteristics of jet array impingement cooling in the quasi-leading-edge channel for steam cooling are very similar to those for air cooling. The difference is that the distribution patterns of the local Nusselt number at the impingement areas of the first five rows of jet holes are kidney-shaped for steam cooling and circular for air cooling. This is because the sizes and distribution positions of the counter-rotating vortex pairs formed on both sides of the jet holes are different for steam cooling and air cooling. Furthermore, the local Nusselt number on the target wall of the quasi-leading-edge channel for steam cooling is obviously higher than that for air cooling. This is because the Pr of steam at a temperature of 474 K and a pressure of 244 kPa is 0.968, which is significantly higher than the Pr of air, which is 0.690 under this condition. It is well known that the wall Nusselt number of a heated channel is roughly proportional to Pr^4. Therefore, the heat transfer effect of jet array impingement cooling in the quasi-leading-edge channel for steam cooling is significantly better than that of air cooling.

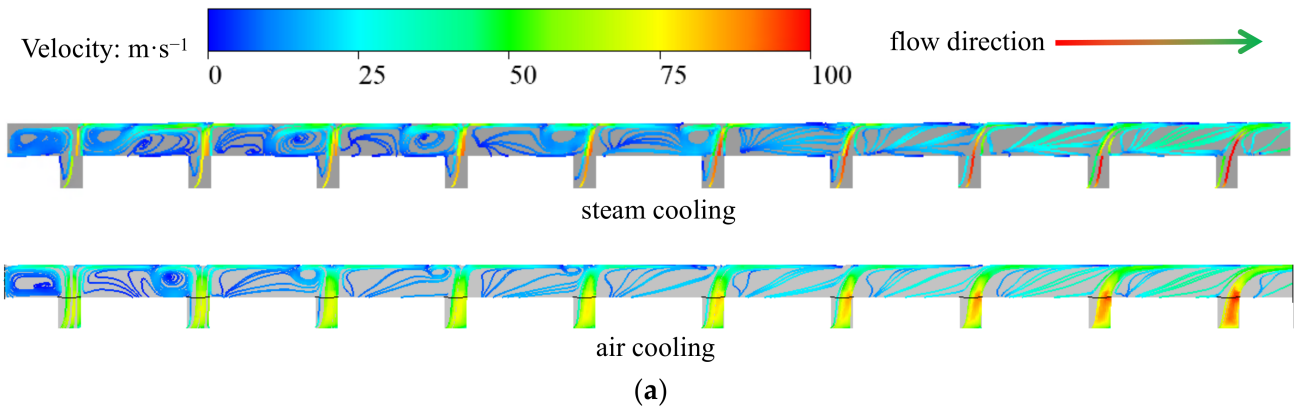

Figure 13. *Cont.*

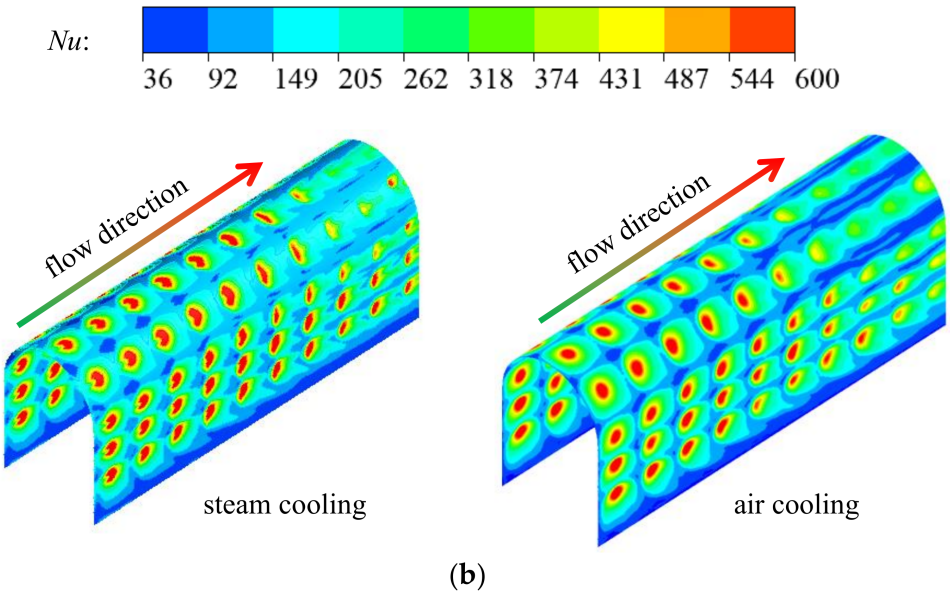

Figure 13. Distributions of flow field and heat transfer under steam cooling and air cooling: (**a**) flow field distributions; (**b**) heat transfer distributions.

Figure 14 shows the comparisons of the pressure loss coefficient, average Nusselt number, and comprehensive thermal coefficient of the quasi-leading-edge channel for steam cooling and air cooling at d/H = 0.7 and S/H = 4. It can be seen from Figure 14a that the variation trends of the pressure loss coefficients with *Re* for jet array impingement cooling in the quasi-leading-edge channel are basically the same for steam cooling and air cooling. As with steam cooling, the increase in *Re* also has little effect on the pressure loss coefficient of the quasi-leading-edge for air cooling. It is worth noting that the pressure loss coefficient in the quasi-leading-edge channel for steam cooling is slightly less than that for air cooling. The maximum difference in pressure loss coefficients in the quasi-leading-edge channel between steam cooling and air cooling is only −0.64%. It can be observed from Figure 14b that the average Nusselt numbers on the target wall of the quasi-leading-edge channel increase with increasing *Re* for both steam cooling and air cooling. Meanwhile, the increase rate of the average Nusselt number of the quasi-leading-edge channel for the air cooling greatly reduces with the increase in *Re*, which is obviously lower than that for the steam cooling. Moreover, the average Nusselt numbers of the quasi-leading-edge channel for the steam cooling are 17.19% to 36.36% higher than those for the air cooling under different *Re*. It can be established from Figure 8c that the comprehensive thermal coefficients of the quasi-leading-edge channel for steam cooling and air cooling both increase with the increase in *Re*. Meanwhile, increasing *Re* makes the gap between the comprehensive thermal coefficients of the quasi-leading-edge channel for steam cooling and air cooling become larger. Additionally, the comprehensive thermal coefficients of the quasi-leading-edge channel for steam cooling are 18.78% to 38.35% higher than those for air cooling when *Re* increases from 10,000 to 60,000. In summary, when compared with air cooling, steam cooling does not increase the pressure loss coefficient of jet array impingement cooling in the quasi-leading-edge channel but can effectively improve the heat transfer performance and comprehensive thermal performance of the quasi-leading-edge channel.

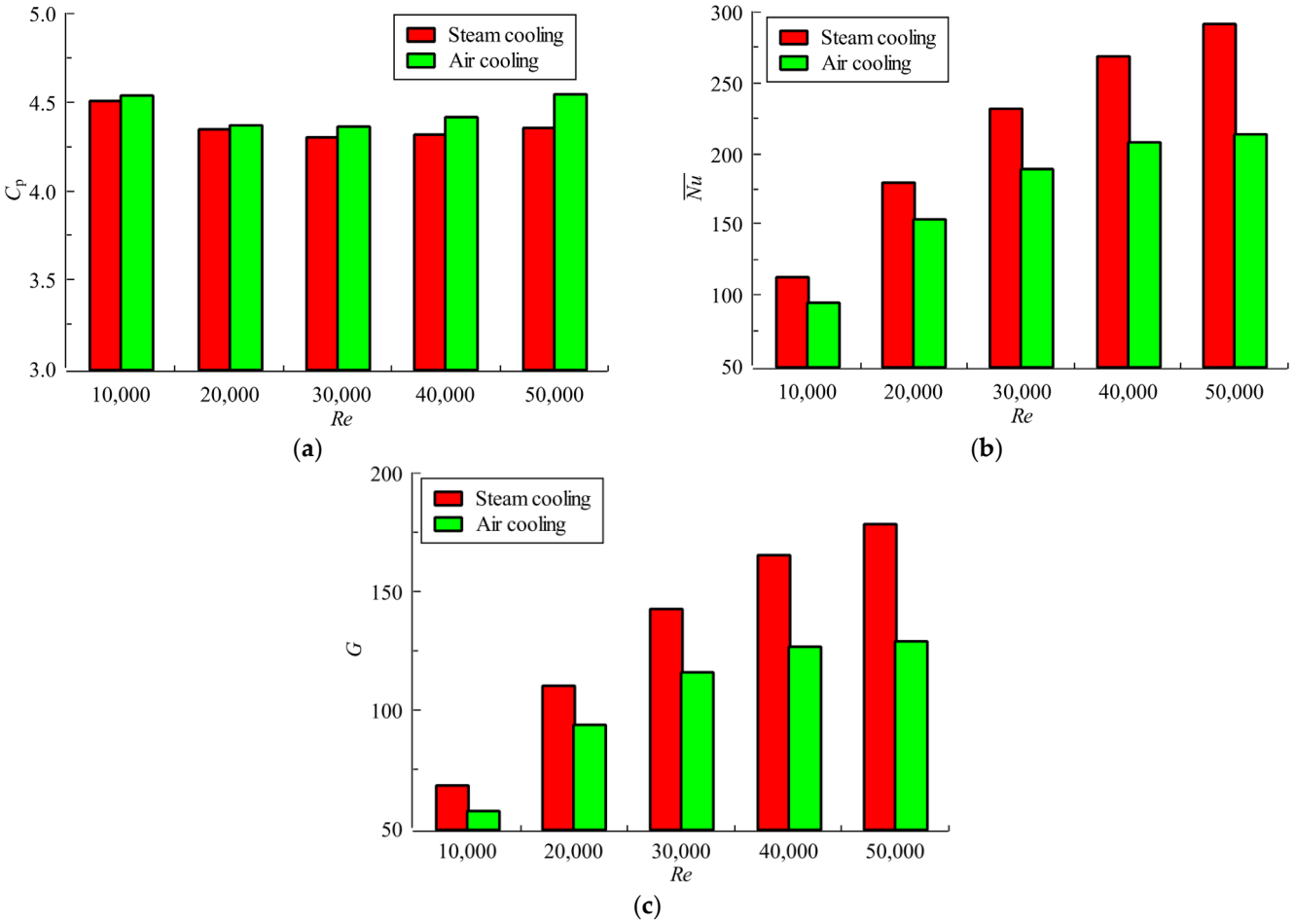

Figure 14. Comparisons of the pressure loss coefficient, average Nusselt number, and comprehensive thermal coefficient of the quasi-leading-edge channel for steam cooling and air cooling: (**a**) pressure loss coefficient; (**b**) average Nusselt number; (**c**) comprehensive thermal coefficient.

4.6. Correlation Fitting

In this section, the empirical correlations of heat transfer coefficients and pressure loss coefficients for jet array impingement cooling in the quasi-leading-edge channel are fitted to facilitate the application of the research results of this study. According to the analysis in Sections 4.1–4.3, the pressure loss coefficient and the average Nusselt number of jet array impingement cooling in the quasi-leading-edge channel monotonically decrease with the increase in *d*/*H*, and monotonously increase with the increase in *S*/*H*. Meanwhile, the change in C_p with the increase in *Re* is very small, and the *Nu* monotonically increases with the increase in *Re*. The comprehensive thermal coefficient *G* of jet array impingement cooling in the quasi-leading-edge channel roughly increases with the increase in *Re* and *S*/*H*, and roughly decreases with the increase in *d*/*H*. In addition, the *Pr* of the cooling medium corresponding to steam cooling and air cooling was also considered when fitting the correlations. Therefore, the correlations of C_p, *Nu*, and *G* with *Re*, *d*/*H*, *S*/*H*, and *Pr* were assumed to be power functions. The general form of the power function is:

$$f = aRe^b(d/H)^c(S/H)^d Pr^e \quad (9)$$

where *f* represents C_p, *Nu*, and *G*; *a*, *b*, *c*, *d*, and *e* are the parameters needed to be fitted.

Based on the results in Figures 6, 7 and 9–12, as well as Equation (9), the empirical correlations of C_p, Nu, and G related to the parameters of Re, d/H, S/H, and Pr were fitted by the Curve_fit module in the SciPy package of Python. The results are as follows:

$$C_p = 0.378Re^{0.005}(d/H)^{-2.799}(S/H)^{1.084}Pr^{0.097} \quad (10)$$

$$Nu = 0.181Re^{0.588}(d/H)^{-1.12}(S/H)^{0.431}Pr^{0.436} \quad (11)$$

$$G = 0.263Re^{0.585}(d/H)^{-0.212}(S/H)^{0.091}Pr^{0.701} \quad (12)$$

The ranges of parameters were: $10{,}000 \leq Re \leq 50{,}000$, $0.5 \leq d/H \leq 0.9$, $2 \leq S/H \leq 6$, and $0.690 \leq Pr \leq 0.968$. The above empirical correlations are applicable to the cooling of the leading edge regions of gas turbine blades with the requirements of high cooling efficiency and low pressure loss.

Figure 15 shows the error distributions of the fitted empirical correlations. As can be seen from Figure 15, the maximum relative errors of C_p correlation, Nu correlation, and G correlation are 15.06%, 13.89%, and −13.41%, and the mean relative errors of C_p correlation, Nu correlation, and G correlation are 7.02%, 6.61%, and 4.72%, respectively. Therefore, the empirical correlations of C_p, Nu, and G fitted in this paper can provide a relatively accurate reference for the prediction of the average Nusselt number, pressure loss coefficient, and comprehensive thermal performance of jet array impingement cooling in the quasi-leading-edge channel.

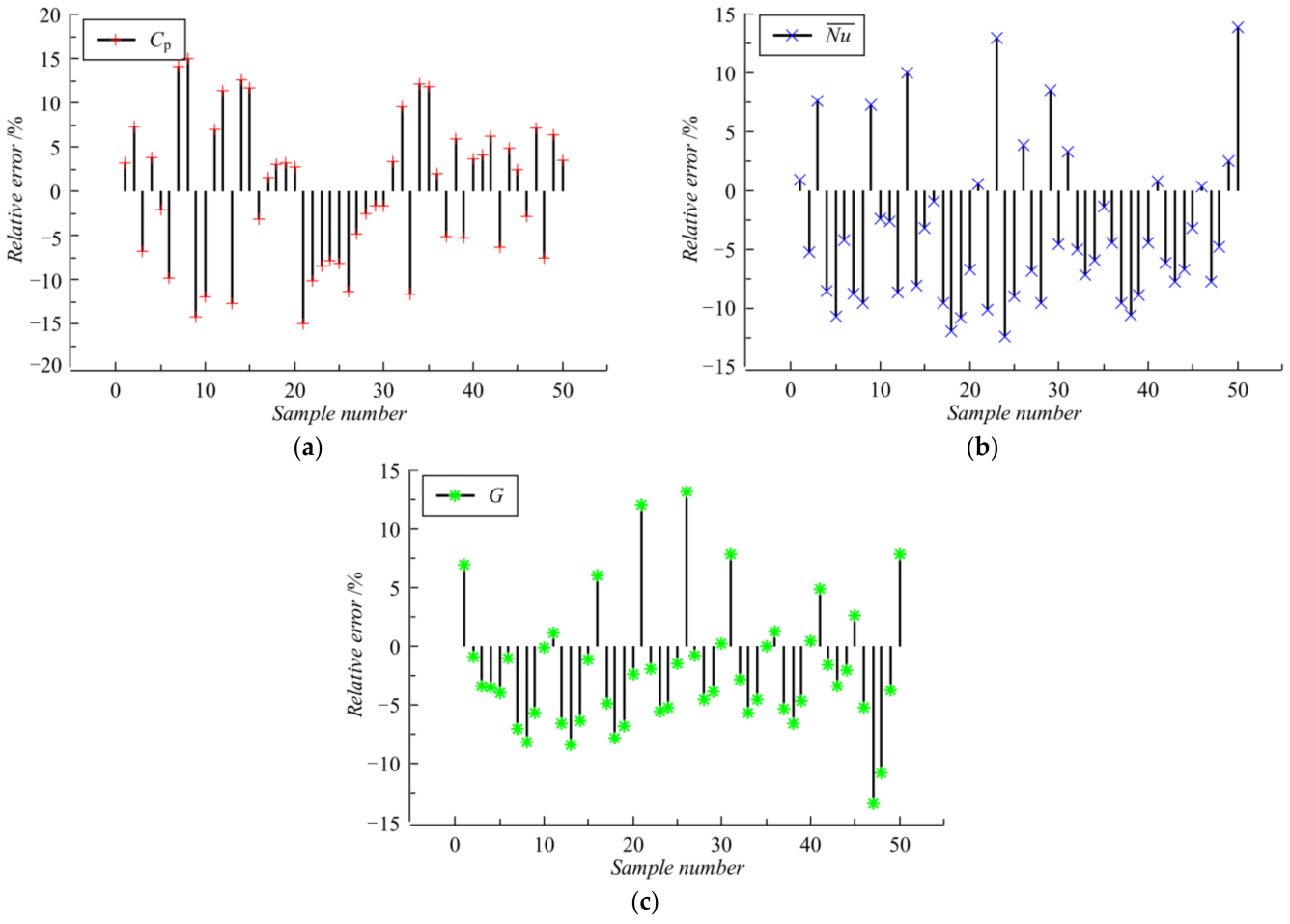

Figure 15. Fitting errors: (**a**) C_p; (**b**) Nu; (**c**) G.

4.7. Parameter Sensitivity Analysis

Sensitivity analysis is a method for studying the degree of influence of changes in input parameters on output parameters. The importance of input parameters to output parameters can be obtained through sensitivity analysis. The greater the sensitivity coefficient, the more important the input parameters are. In this investigation, the Sobol method, which is a widely used global sensitivity analysis method based on variance decomposition, was used to accomplish parameter sensitivity analysis for jet array impingement cooling in the quasi-leading-edge channel. The principle of the Sobol method is to calculate the contribution of each input parameter to the variance of each output parameter so as to determine the relative influence level of each input parameter on the output parameters. Therefore, this method can robustly and reliably calculate the sensitivity caused by the interaction effect between input parameters in the highly nonlinear model [37]. The Sobol method can calculate the first-order, second-order, and total sensitivity coefficients of each input parameter. This investigation focused on the overall influence level of each input parameter of the quasi-leading-edge channel, therefore only the analysis of the total sensitivity coefficient S_{T} of each input parameter was carried out. The calculation formula of the total sensitivity coefficient $S_{\mathrm{T}i}$ for the ith input parameter is [37]:

$$S_{\mathrm{T}i} = \frac{\sum_{n=1}^{N'} \left(f(\mathbf{A}_n) - f(\mathbf{A}_{B,n}^{i})\right)^2 / 2N'}{\sigma_y^2} \tag{13}$$

where N' is the number of sample points; both A and B are the $N' \times I$ matrices, which are generated by the Sobol method in Python; n represents the nth row in the matrix; I is the number of input parameters; σ_y^2 is the variance of the output parameter.

Based on Equations (10)–(13), the parameter sensitivity analysis of flow performance, heat transfer performance, and comprehensive thermal performance of jet array impingement cooling in the quasi-leading-edge channel to *Re*, *d/H*, *S/H*, and *Pr* was carried out. The results of the sensitivity analysis are shown in Figure 16. As can be seen from Figure 16, the pressure loss coefficient of the quasi-leading-edge channel is most sensitive to the change in *d/H*, followed by the changes in *S/H* and *Pr*, while it is not sensitive to the change in *Re*. This is because the pressure difference between the channel inlet and outlet as well as the square of the inlet velocity both increase with the increase in *Re*, which results in a small change in the pressure loss coefficient with the increase in *Re*. The average Nusselt number of the quasi-leading-edge channel is most sensitive to the change in *Re*, followed by the changes in *d/H* and *S/H*, and is least sensitive to the change in *Pr*. The comprehensive thermal coefficient of the quasi-leading-edge channel is also the most sensitive to the change in *Re*, followed by the change in *Pr*, and is least sensitive to the changes in *d/H* and *S/H*. It can also be seen from Figure 16 that the sensitivity coefficients of the wall average Nusselt number and the comprehensive thermal coefficient of the quasi-leading-edge channel to *Re* are both relatively high, and are much larger than the sensitivity coefficient of the pressure loss coefficient to *Re*. This indicates that the change in the *Re* has much greater influence on the heat transfer performance and comprehensive thermal performance of the quasi-leading-edge channel than on the flow performance of the channel. The sensitivity coefficients of the wall average Nusselt number and the comprehensive thermal coefficient of the quasi-leading-edge channel to the *d/H* and *S/H* are obviously smaller than the sensitivity coefficients of the pressure loss coefficient to the *d/H* and *S/H*. It shows that the changes in the *d/H* and *S/H* have a smaller influence on the heat transfer performance and comprehensive thermal performance of the quasi-leading-edge channel than on the flow performance of the channel. The sensitivity coefficients of the pressure loss coefficient, wall average Nusselt number, and comprehensive thermal coefficient of the quasi-leading-edge channel to the *Pr* are all small, implying that the influence levels of steam cooling on the flow performance, heat transfer performance, and comprehensive thermal performance of the quasi-leading-edge channel are relatively small when taking air cooling as the reference.

In summary, when the heat transfer performance of jet array impingement cooling in the quasi-leading-edge channel is expected to be enhanced, the two parameters of *Re* and *d/H* are the most important. When the pressure loss of jet array impingement cooling of the quasi-leading-edge channel is expected to be reduced, most attention should be paid to the parameters of *d/H* and *S/H*. When the comprehensive thermal performance of the quasi-leading-edge channel is expected to be improved, *Re* is most important.

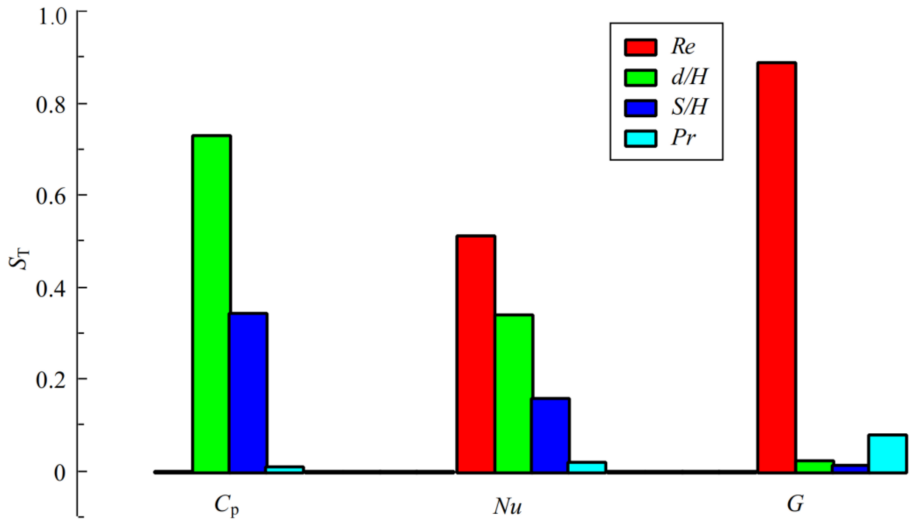

Figure 16. Distribution of the total sensitivity coefficients.

5. Conclusions

In this investigation, the flow and heat transfer characteristics of jet array impingement cooling in the quasi-leading-edge channel of a gas turbine blade were numerically analyzed. The main findings are as follows:

(1) The change in *Re* has relatively little effect on the pressure loss coefficient of jet array impingement cooling in the quasi-leading-edge channel. When *Re* increases from 10,000 to 60,000 under different *d/H* and *S/H*, the average Nusselt number of the quasi-leading-edge channel increases by 1.59 to 1.91 times and the comprehensive thermal coefficient of the quasi-leading-edge channel increases by 1.62 to 1.86 times.

(2) When the *d/H* changes from 0.5 to 0.9 at different *Re*, the pressure loss coefficient in the quasi-leading-edge channel decreases by 76% to 79% and the average Nusselt number of the target wall decreases by about 45% to 49%. When the *S/H* increases from 2 to 6 at different *Re*, the pressure loss coefficient in the channel increases by about 1.64 to 1.92 times and the average Nusselt number of the target wall increases by 54% to 64%.

(3) The pressure loss coefficient in the quasi-leading-edge channel can be reduced by increasing the jet hole diameter and reducing the jet hole spacing. The heat transfer effect of the target wall can be improved by reducing the jet hole diameter and increasing the jet hole spacing. The comprehensive thermodynamic coefficient reaches its maximum values at $d/H = 0.6$ for lower Reynolds numbers and at $S/H = 5$ for higher Reynolds numbers.

(4) The pressure loss coefficient in the quasi-leading-edge channel for steam cooling is slightly less than that for air cooling. The average Nusselt numbers and comprehensive thermal coefficients of the quasi-leading-edge channel for steam cooling are 17.19% to 36.36% and 18.78% to 38.35% higher than those for air cooling under different *Re*.

(5) The pressure loss coefficient of the quasi-leading-edge channel is most sensitive to the change in *d/H*, followed by the changes in *S/H* and *Pr*, while it is not sensitive to the

change in *Re*. The average Nusselt number of the quasi-leading-edge channel is most sensitive to the change in *Re*, followed by the changes in *d/H* and *S/H*, and is least sensitive to the change in *Pr*. The comprehensive thermal coefficient of the channel is most sensitive to the change in *Re*, followed by the change in *Pr*, and is least sensitive to the changes in *d/H* and *S/H*.

(6) When the heat transfer performance of jet array impingement cooling in the quasi-leading-edge channel is expected to be enhanced, the two parameters of *Re* and *d/H* are the most important. When the pressure loss of the quasi-leading-edge channel is expected to be reduced, most attention should be paid to the parameters of *d/H* and *S/H*. When the comprehensive thermal performance of the quasi-leading-edge channel is expected to be improved, *Re* is most important.

Author Contributions: Conceptualization, L.X. (Lei Xi). and J.G.; methodology, L.X. (Lei Xi); validation, L.X. (Lei Xi), J.G. and L.X. (Liang Xu); formal analysis, Q.R.; investigation, Z.Z.; resources, J.G.; data curation, Z.Z.; writing—original draft preparation, L.X. (Lei Xi); writing—review and editing, Z.Z.; visualization, Q.R.; supervision, Y.L. and L.X. (Lei Xi); project administration, Y.L. and J.G. All authors have read and agreed to the published version of the manuscript.

Funding: The authors would like to express their sincere gratitude to the China Postdoctoral Science Foundation (2021M702573) and National Natural Science Foundation of China (51876157) for providing financial support for this work.

Institutional Review Board Statement: Not applicable.

Informed Consent Statement: Not applicable.

Data Availability Statement: Not applicable.

Conflicts of Interest: The authors declare no conflict of interest.

Nomenclature

C_p	pressure loss coefficient
d	diameter of jet hole, mm
D	equivalent diameter of the plug-in channel, mm
G	comprehensive thermal coefficient
H	jet impinging distance, mm
L	channel length, mm
Nu	local Nusselt number
$\overline{Nu}$	average Nusselt number
Pr	Prandtl number
p_{in}	channel inlet pressure, Pa
p_{out}	channel outlet pressure, Pa
q	wall heat flux, $W \cdot m^{-2}$
Re	Reynolds number
s	circumferential distance, mm
S	axial jet hole spacing
S_T	total sensitivity coefficient
T_{in}	inlet temperature, K
T_w	local wall temperature, K
u	inlet velocity, $m \cdot s^{-1}$
Greek symbols	
λ	thermal conductivity of the coolant, $W \cdot m^{-1} \cdot K^{-1}$
ρ	density of the coolant, $kg \cdot m^{-3}$
v	kinematic viscosity of the coolant, $m^2 \cdot s^{-1}$
φ	absolute uncertainty
μ	dynamic viscosity, Pa·s

References

1. Xi, L.; Xu, L.; Gao, J.; Zhao, Z.; Li, Y. Cooling performance analysis and structural parameter optimization of X-type truss array channel based on neural networks and genetic algorithm. *Int. J. Heat Mass Transf.* **2022**, *186*, 122452. [CrossRef]
2. Hussain, L.; Khan, M.M.; Masud, M.; Ahmed, F.; Rehman, Z.; Amanowicz, Ł.; Rajski, K. Heat Transfer Augmentation through Different Jet Impingement Techniques: A State-of-the-Art Review. *Energies* **2021**, *14*, 6458. [CrossRef]
3. Ekkad, S.V.; Singh, P. A modern review on jet impingement heat transfer methods. *J. Heat Transf.* **2021**, *143*, 064001. [CrossRef]
4. Bradbury, L.J.S. The structure of a self-preserving turbulent plane jet. *J. Fluid Mech.* **1965**, *23*, 31–64. [CrossRef]
5. Kercher, D.M. Heat transfer by a square array of round air jets impinging perpendicular to a flat surface including the effect of spent air. *J. Eng. Gas Turbines Power* **1970**, *92*, 73–82. [CrossRef]
6. Liu, L.; Zhu, X.; Liu, H.; Du, Z. Effect of tangential jet impingement on blade leading edge impingement heat transfer. *Appl. Therm. Eng.* **2018**, *130*, 1380–1390. [CrossRef]
7. Long, J.; New, T.H. Vortical structures and behaviour of an elliptic jet impinging upon a convex cylinder. *Exp. Therm. Fluid Sci.* **2019**, *100*, 292–310. [CrossRef]
8. Nguyen, D.T.; Maher, B.; Hassan, Y. Effects of nozzle pressure ratio and nozzle-to-plate distance to flowfield characteristics of an under-expanded jet impinging on a flat surface. *Aerospace* **2019**, *6*, 4. [CrossRef]
9. Xu, L.; Yang, T.; Sun, Y.; Xi, L.; Gao, J.; Li, Y. Flow and heat transfer characteristics of a swirling impinging jet issuing from a threaded nozzle of 45 degrees. *Energies* **2021**, *14*, 8412. [CrossRef]
10. Dutta, S.; Singh, P. Opportunities in jet-impingement cooling for gas-turbine engines. *Energies* **2021**, *14*, 6587. [CrossRef]
11. Deng, Q.; Wang, H.; He, W.; Feng, Z. Cooling characteristic of a wall jet for suppressing crossflow effect under conjugate heat transfer condition. *Aerospace* **2022**, *9*, 29. [CrossRef]
12. Yang, X.; Wu, H.; Feng, Z. Jet impingement heat transfer characteristics with variable extended jet holes under strong crossflow conditions. *Aerospace* **2022**, *9*, 44. [CrossRef]
13. Patil, V.S.; Vedula, R.P. Local heat transfer for jet impingement onto a concave surface including injection nozzle length to diameter and curvature ratio effects. *Exp. Therm. Fluid Sci.* **2018**, *92*, 375–389. [CrossRef]
14. Wang, N.; Chen, A.F.; Zhang, M.; Han, J.C. Turbine blade leading edge cooling with one row of normal or tangential impinging jets. *J. Heat Transf.* **2018**, *140*, 62201. [CrossRef]
15. Li, Z.; Liu, J.; Zhou, W.; Liu, Y.; Wen, X. Experimental investigation of flow dynamics of sweeping jets impinging upon confined concave surfaces. *Int. J. Heat Mass Transf.* **2019**, *142*, 118457. [CrossRef]
16. Lyu, Y.; Zhang, J.; Liu, X.; Shan, Y. Experimental study of single-row chevron-jet impingement heat transfer on concave surfaces with different curvatures. *Chin. J. Aeronaut.* **2019**, *32*, 2275–2285. [CrossRef]
17. Lyu, Y.; Zhang, J.; Wang, B.; Tan, X. Convective heat transfer on flat and concave surfaces subjected to an impinging jet form lobed nozzle. *Sci. China Technol. Sci.* **2020**, *63*, 116–127. [CrossRef]
18. Kura, T.; Fornalik-Wajs, E.; Wajs, J.; Kenjeres, S. Curved surface minijet impingement phenomena analysed with ζ-f turbulence model. *Energies* **2021**, *14*, 1846. [CrossRef]
19. Xu, L.; Zhao, X.; Xi, L.; Ma, Y.; Gao, J.; Li, Y. Large-eddy simulation study of flow and heat transfer in swirling and non-swirling impinging jets on a semi-cylinder concave target. *Appl. Sci.* **2021**, *11*, 7167. [CrossRef]
20. Xu, L.; Yun, X.; Xi, L.; Gao, J.; Yang, T.; Li, Y. Heat transfer characteristics of single row of jets issuing from screw-thread nozzles impinging on a concave surface. *Case Stud. Therm. Eng.* **2021**, *28*, 101590. [CrossRef]
21. Qiu, D.; Luo, L.; Zhao, Z.; Wang, S.; Wang, Z.; Sundén, B. On heat transfer and flow characteristics of jets impingement on a concave surface with varying pin-fin arrangements. *Int. J. Therm. Sci.* **2021**, *170*, 107163. [CrossRef]
22. Tepe, A.Ü. Numerical investigation of a novel jet hole design for staggered array jet impingement cooling on a semicircular concave surface. *Int. J. Therm. Sci.* **2021**, *162*, 106792. [CrossRef]
23. Forster, M.; Weigand, B. Experimental and numerical investigation of jet impingement cooling onto a concave leading edge of a generic gas turbine blade. *Int. J. Therm. Sci.* **2021**, *164*, 106862. [CrossRef]
24. Seifi, Z.; Nazari, M.R.; Khalaji, E. 2D numerical simulation of impinging jet onto the concave surface by k-w-v2-f turbulence model. *Heat Mass Transf.* **2017**, *53*, 59–72. [CrossRef]
25. Hadipour, A.; Zargarabadi, M.R. Heat transfer and flow characteristics of impinging jet on a concave surface at small nozzle to surface distances. *Appl. Therm. Eng.* **2018**, *138*, 534–541. [CrossRef]
26. Hadipour, A.; Zargarabadi, M.R.; Mohammadpour, J. Effects of a triangular guide rib on flow and heat transfer in a turbulent jet impingement on an asymmetric concave surface. *Phys. Fluids* **2020**, *32*, 075112. [CrossRef]
27. Ravanji, A.; Zargarabadi, M.R. Effects of elliptical pin-fins on heat transfer characteristics of a single impinging jet on a concave surface. *Int. J. Heat Mass Transf.* **2020**, *152*, 119532. [CrossRef]
28. Huang, H.; Sun, T.; Li, N.; Zhang, G. Sensitization of the modified SST model to the swirling and curvature for turbulent impinging jet heat transfer. *Int. J. Heat Mass Transf.* **2022**, *182*, 121980. [CrossRef]
29. Li, X.; Gaddis, J.L.; Wang, T. Mist/steam heat transfer in confined slot jet impingement. *J. Turbomach.* **2001**, *123*, 161–167. [CrossRef]
30. Wang, T.; Dhanasekaran, T.S. Calibration of a computational model to predict mist/steam impinging jets cooling with an application to gas turbine blades. *J. Heat Transf.* **2010**, *132*, 122201. [CrossRef]

31. Wang, T.; Dhanasekaran, T.S. Model verification of mist/steam cooling with jet impingement onto a concave surface and prediction at elevated operating conditions. *J. Turbomach.* **2012**, *134*, 021016. [CrossRef]
32. Xu, L.; Shuai, Z.; Wang, W.; Gao, J.; Gao, T. Numerical study of on cooling performance for multi-holes steam jet in the internal channel of a hollow turbine blade in international heat transfer conference digital library. In Proceedings of the 15th International Heat Transfer Conference, IHTC-15At, Kyoto, Japan, 10–15 August 2014; Begel House Inc.: Kyoto, Japan, 2014. [CrossRef]
33. Alhajeri, H.M.; Almutairi, A.; Alenezi, A.; Gamil, A.A.; Al-Hajeri, M.H. Effect of mist/steam uniformity on heat transfer characteristics in unconfined jet impingement. *Appl. Therm. Eng.* **2021**, *186*, 116299. [CrossRef]
34. Diop, S.N.; Dieng, B.; Warore, A.; Mbodj, S. A study on heat transfer characteristics by impinging jet within a few amounts of mist. *Int. J. Thermofluids* **2022**, *13*, 100130. [CrossRef]
35. Xu, L.; Wang, W.; Gao, T.; Shi, X.; Gao, J.; Liang, W. Experimental study on cooling performance of a steam-cooled turbine blade with five internal cooling smooth channels. *Exp. Therm. Fluid Sci.* **2014**, *58*, 180–187. [CrossRef]
36. Zhang, Y.; Liu, Y.; Zhang, Y.; Wang, W.; Han, Y. Hypersonic boundary layer flow and heat transfer analysis of compressible fluid over a permeable wall with gas injection. *Int. Commun. Heat Mass* **2021**, *129*, 105688. [CrossRef]
37. Yang, H.; Wen, J.; Wang, S.; Li, Y.; Tu, J.; Cai, W. Sobol sensitivity analysis for governing variables in design of a plate-fin heat exchanger with serrated fins. *Int. J. Heat Mass Transf.* **2017**, *115*, 871–881. [CrossRef]